AFRL-AFOSR-VA-TR-2015-0331

Method of Lines Transpose an Implicit Vlasov Maxwell Solver for Plasmas

Andrew Christlieb
MICHIGAN STATE UNIV EAST LANSING

04/17/2015
Final Report

Air Force Research Laboratory
AF Office Of Scientific Research (AFOSR)/ RTA2
Arlington, Virginia 22203
Air Force Materiel Command

REPORT DOCUMENTATION PAGE

Form Approved
OMB No. 0704-0188

PLEASE DO NOT RETURN YOUR FORM TO THE ABOVE ORGANIZATION.

1. REPORT DATE *(DD-MM-YYYY)*	2. REPORT TYPE	3. DATES COVERED *(From - To)*
14/04/2015	Finel Report	June 2010- Jan 2015

4. TITLE AND SUBTITLE

Method of Lines Transpose an Implicit Vlasov Maxwell Solver for Plasmas
(A new Implicit Particle In Cell Code)

5a. CONTRACT NUMBER
FA9550-11-1-0281

5b. GRANT NUMBER

5c. PROGRAM ELEMENT NUMBER

6. AUTHOR(S)

Andrew Chrisltlieb

5d. PROJECT NUMBER

5e. TASK NUMBER

5f. WORK UNIT NUMBER

7. PERFORMING ORGANIZATION NAME(S) AND ADDRESS(ES)

Michigan State University
Department of Mathematics
619 Red Cedar Road

8. PERFORMING ORGANIZATION REPORT NUMBER

9. SPONSORING/MONITORING AGENCY NAME(S) AND ADDRESS(ES)

Air Force Office of Scientific Research
875 N. Randolph St., Rm 3112
Arlington, VA 22203

10. SPONSOR/MONITOR'S ACRONYM(S)

11. SPONSOR/MONITOR'S REPORT NUMBER(S)

12. DISTRIBUTION/AVAILABILITY STATEMENT

Distribution A

13. SUPPLEMENTARY NOTES

14. ABSTRACT

We present a new particle-in-cell (PIC) method for the simulation of plasmas based on a recently developed, unconditionally stable solver for the wave equation. This method is not subject to a CFL restriction, limiting the ratio of the time step size to the spatial step size, typical of explicit methods, while maintaining computational cost and code complexity comparable to such explicit schemes. We describe the implementation in one and two dimensions for both electrostatic and electromagnetic cases, and present the results of several standard test problems, showing good agreement with theory with time step sizes much larger than allowed by typical CFL restrictions.

15. SUBJECT TERMS

Method of Lines Transpose , Implicit Wave Solver, Particle In Cell,
Successive Convolution, Alternating Direction Implicit Splitting

16. SECURITY CLASSIFICATION OF:			17. LIMITATION OF ABSTRACT	18. NUMBER OF PAGES	19a. NAME OF RESPONSIBLE PERSON
a. REPORT	b. ABSTRACT	c. THIS PAGE			Andrew Chrisltlieb
U	U	U	UU	39	19b. TELEPHONE NUMBER *(Include area code)* 5173533831

Reset

Standard Form 298 (Rev. 8/98)
Prescribed by ANSI Std. Z39.18
Adobe Professional 7.0

INSTRUCTIONS FOR COMPLETING SF 298

1. REPORT DATE. Full publication date, including day, month, if available. Must cite at least the year and be Year 2000 compliant, e.g. 30-06-1998; xx-06-1998; xx-xx-1998.

2. REPORT TYPE. State the type of report, such as final, technical, interim, memorandum, master's thesis, progress, quarterly, research, special, group study, etc.

3. DATES COVERED. Indicate the time during which the work was performed and the report was written, e.g., Jun 1997 - Jun 1998; 1-10 Jun 1996; May - Nov 1998; Nov 1998.

4. TITLE. Enter title and subtitle with volume number and part number, if applicable. On classified documents, enter the title classification in parentheses.

5a. CONTRACT NUMBER. Enter all contract numbers as they appear in the report, e.g. F33615-86-C-5169.

5b. GRANT NUMBER. Enter all grant numbers as they appear in the report, e.g. AFOSR-82-1234.

5c. PROGRAM ELEMENT NUMBER. Enter all program element numbers as they appear in the report, e.g. 61101A.

5d. PROJECT NUMBER. Enter all project numbers as they appear in the report, e.g. 1F665702D1257; ILIR.

5e. TASK NUMBER. Enter all task numbers as they appear in the report, e.g. 05; RF0330201; T4112.

5f. WORK UNIT NUMBER. Enter all work unit numbers as they appear in the report, e.g. 001; AFAPL30480105.

6. AUTHOR(S). Enter name(s) of person(s) responsible for writing the report, performing the research, or credited with the content of the report. The form of entry is the last name, first name, middle initial, and additional qualifiers separated by commas, e.g. Smith, Richard, J, Jr.

7. PERFORMING ORGANIZATION NAME(S) AND ADDRESS(ES). Self-explanatory.

8. PERFORMING ORGANIZATION REPORT NUMBER. Enter all unique alphanumeric report numbers assigned by the performing organization, e.g. BRL-1234; AFWL-TR-85-4017-Vol-21-PT-2.

9. SPONSORING/MONITORING AGENCY NAME(S) AND ADDRESS(ES). Enter the name and address of the organization(s) financially responsible for and monitoring the work.

10. SPONSOR/MONITOR'S ACRONYM(S). Enter, if available, e.g. BRL, ARDEC, NADC.

11. SPONSOR/MONITOR'S REPORT NUMBER(S). Enter report number as assigned by the sponsoring/ monitoring agency, if available, e.g. BRL-TR-829; -215.

12. DISTRIBUTION/AVAILABILITY STATEMENT. Use agency-mandated availability statements to indicate the public availability or distribution limitations of the report. If additional limitations/ restrictions or special markings are indicated, follow agency authorization procedures, e.g. RD/FRD, PROPIN, ITAR, etc. Include copyright information.

13. SUPPLEMENTARY NOTES. Enter information not included elsewhere such as: prepared in cooperation with; translation of; report supersedes; old edition number, etc.

14. ABSTRACT. A brief (approximately 200 words) factual summary of the most significant information.

15. SUBJECT TERMS. Key words or phrases identifying major concepts in the report.

16. SECURITY CLASSIFICATION. Enter security classification in accordance with security classification regulations, e.g. U, C, S, etc. If this form contains classified information, stamp classification level on the top and bottom of this page.

17. LIMITATION OF ABSTRACT. This block must be completed to assign a distribution limitation to the abstract. Enter UU (Unclassified Unlimited) or SAR (Same as Report). An entry in this block is necessary if the abstract is to be limited.

Method of Lines Transpose an Implicit Vlasov Maxwell Solver for Plasmas

ANDREW CHRISTLIEB

Abstract. We propose a new particle-in-cell (PIC) method for the simulation of plasmas based on a recently developed, unconditionally stable solver for the wave equation. This method is not subject to a CFL restriction, limiting the ratio of the time step size to the spatial step size, typical of explicit methods, while maintaining computational cost and code complexity comparable to such explicit schemes. We describe the implementation in one and two dimensions for both electrostatic and electromagnetic cases, and present the results of several standard test problems, showing good agreement with theory with time step sizes much larger than allowed by typical CFL restrictions.

1. Introduction

This is a final report for the AFOSR grant "Method of Lines Transpose an Implicit Vlasov Maxwell Solver for Plasmas". The contact number was FA9550-11-1-0281. The grant was concerned with the development of a new approach for developing A-sable high order waves solvers for combination with particle methods. The work on the wave solver has been published and can be found in [8, 7, 9]. In this report, we detail our first attempt at turning this wave solver into an implicit method for particle-in-cell, as well as go over a host of example problems in 1D and 2D. This work was in conjunction with two former post docs, funded by this grant, Dr. Yaman Güçlü and Dr. Matt Caulesy, as well as my student, Mr. Eric Wolf, who's thesis is the subject of this work. In addition, we have ben collaborating with Dr. Matthew Bettencourt from Sandia National Lab, who has ben part of the large scale effort at Sandia to develop an implicit particle method. These ideas can be extended to methods for Pseudo Differential Operators (PDO), and my current student, Ms. Hana Cho, who is starting to work in this area.

Collisionless plasmas - systems of charged particles interacting through electromagnetic fields - are modelled by the Vlasov-Maxwell system of partial differential equations (PDEs), which couple Maxwell's equations, describing the evolution of the electric and magnetic fields $\mathbf{E}$ and $\mathbf{B}$, to Vlasov equations, a type of hyperbolic PDE describing the evolution of the phase-space distribution functions (DFs) f_s of the various species s of charged particles. Particle-in-cell (PIC) methods [4, 18, 38], in development and use since the 1960s and a primary tool in the computer simulation of plasmas, combine an Eulerian description of the fields with a Lagrangian description of the DFs; that is, fields are evolved on a fixed mesh, while DFs are represented by moving particles whose trajectories are characteristics of the corresponding Vlasov equation. Thus, PIC methods require a method to compute the fields on a mesh and a method to compute particle trajectories, as well as interpolation tools to provide for their coupling. This work focuses on a new method for the computation of the fields, along with associated interpolation techniques.

Under the Lorenz gauge condition, Maxwell's equations reduce to uncoupled wave equations for the scalar and vector potentials, Φ and $\mathbf{A}$. Recently, a novel method for the solution of the wave equation has been developed [8, 7, 9], based on the Method of Lines Transpose (MOLT), dimensional splitting and an efficient 1D integral solution method, which is unconditionally stable (or A-stable) - that is, it is not subject to the Courant-Friedrichs-Lewy (CFL) restriction limiting the ratio of the temporal step size to the spatial step size, typical of widely used explicit methods. In this work, we apply this method to the uncoupled wave equations for Φ and $\mathbf{A}$ to solve Maxwell's equations with a method comparable in computational cost and complexity of code to explicit methods such as the well-known Yee scheme [39, 36], but without introducing a CFL restriction based on the speed of light as in such explicit methods. In conjunction with an appropriate description of particles, we seek to develop a PIC method that retains the simplicity of explicit finite-difference-based methods while eliminating this CFL restriction.

We demonstrate the application of our method to both electrostatic and electromagnetic problems. In the non-relativistic, zero-magnetic field limit, it is typical to make the electrostatic approximation, $\mathbf{E} = -\nabla\Phi$, $-\nabla^2\Phi = \rho/\epsilon_0$, simplifying the Vlasov-Maxwell system to the Vlasov-Poisson system. Correspondingly, in this work we consider the same non-relativistic, zero-magnetic field limit, and drop $\mathbf{A}$ and the corresponding wave equations from our model. When particle velocities are small compared to the speed of light, we argue that this model, which we term the Vlasov-Wave model due to the replacement of the Poisson equation with a wave equation, will agree approximately with the usual electrostatic Vlasov-Poisson model. We present numerical results applying our method to several standard electrostatic test problems in one and two dimensions, showing agreement with the predictions of linear theory for the electrostatic model. We apply our method to a fully electromagnetic beam pinch problem in two dimensions. It is well known that an electromagnetic PIC method must satisfy a discrete form of Gauss' law ($\nabla \cdot \mathbf{E} = \rho/\epsilon_0$) to prevent serious numerical errors related to the violation of charge conservation [26]. In this work, we obtain solutions that satisfy exactly discrete forms of Gauss' law for the electric field and the divergence-free condition for the magnetic field through a staggered grid approach, adapted from the well-known Yee grid [39], with a Poisson equation formulation for the scalar potential. In addition to eliminating the CFL restriction, the wave solver method used in this work offers the handling of complex boundary geometry in a Cartesian grid without using a staircasing approximation [7, 37], and can be extended to higher-order accuracy [9], features that will be incorporated into our PIC method in future work.

Building on prior work on unconditionally stable ADI-FDTD schemes for Maxwell's equations [41, 40, 28, 23], unconditionally stable ADI-FDTD methods for Maxwell's equations that conserve the divergence of the discrete electric and magnetic fields were incorporated into PIC methods in [35]. Future work will compare our method to this approach in the context of PIC methods.

In most PIC methods, further stability restrictions also apply, the most restrictive often being the need to resolve the electron plasma period. Our method, making use of explicit algorithms for advancing particles, is subject to such restriction. In problems where time scales much longer than the electron plasma period are of primary interest and dynamics on the scale of the electron plasma period can be safely underresolved - for instance, in certain problems in the study of ion dynamics - it is desirable to take a much larger time step than

prescribed by the plasma period stability restriction. Since years ago [14, 22], and with a recent resurgence [11], it has been sought to develop implicit PIC algorithms that are not subject to the stability restriction based on the plasma period. An ultimate challenge for our method would be synthesis with a suitable implicit particle integration scheme to achieve a practical fully implicit method, eliminating the stability restriction based on the plasma period as well as the field-based CFL restriction. However, that is beyond the scope of the present work.

2. Physical Models

The self-consistent evolution of an single species plasma is described by the Vlasov-Maxwell system, given in the SI system of units by

$$\frac{\partial f}{\partial t} + \mathbf{v} \cdot \nabla_{\mathbf{x}} f + \frac{q}{m} (\mathbf{E} + \mathbf{v} \times \mathbf{B}) \cdot \nabla_{\mathbf{v}} f = 0$$

$$\epsilon_0 \mu_0 \frac{\partial \mathbf{E}}{\partial t} = \nabla \times \mathbf{B} - \mu_0 \mathbf{J} \qquad \frac{\partial \mathbf{B}}{\partial t} = -\nabla \times \mathbf{E}$$
$$\nabla \cdot \mathbf{E} = \rho/\varepsilon_0 \qquad \nabla \cdot \mathbf{B} = 0$$

$$\rho(\mathbf{x}, t) = q \int_{\mathbf{v}} f(\mathbf{x}, \mathbf{v}, t)\, d\mathbf{v}, \quad \mathbf{J} = q \int_{\mathbf{v}} \mathbf{v} f(\mathbf{x}, \mathbf{v}, t)\, d\mathbf{v}$$

where $f(\mathbf{x}, \mathbf{v}, t)$ is the phase-space distribution function, q is the charge and m is the mass of a particle, $\mathbf{E}(\mathbf{x}, t)$ is the electric field, $\mathbf{B}(\mathbf{x}, t)$ is the magnetic field, $\rho(\mathbf{x}, t)$ is the charge density (and ρ_B represents a static uniform background charge distribution), $\mathbf{J}(\mathbf{x}, t)$ is the current density, ε_0 is the electric permittivity of the vacuum, and μ_0 is the magnetic permability of the vacuum. (Boldface variables are to stand for vector quantities, while nonboldface variables are to stand for scalar quantities.)

In the limit, in an appropriate sense, of $|\mathbf{v}|/c \to 0$ (where $c = 1/\sqrt{\varepsilon_0 \mu_0}$ is the speed of light in vacuum) and in the absence of magnetic fields, the Vlasov-Maxwell system reduces to the Vlasov-Poisson system:

$$\frac{\partial f}{\partial t} + \mathbf{v} \cdot \nabla_{\mathbf{x}} f - \frac{q}{m} \nabla \Phi \cdot \nabla_{\mathbf{v}} f = 0$$

$$-\Delta \Phi = \rho/\varepsilon_0, \quad \rho(\mathbf{x}, t) = q \int_{\mathbf{v}} f(\mathbf{x}, \mathbf{v}, t)\, d\mathbf{v}$$

The Vlasov-Maxwell and Vlasov-Poisson models have been widely studied, and many numerical methods have been developed to solve them, such as electrostatic and electromagnetic PIC methods [4, 18, 13, 27, 17], as well as Eulerian methods [12, 16, 31, 1]. Instead of solving either of these systems directly, we seek to develop a semi-implicit approach for the fields based on a vector potential formulation. Under the Lorenz gauge condition,

$$\frac{1}{c^2} \frac{\partial \Phi}{\partial t} + \nabla \cdot \mathbf{A} = 0,$$

Maxwell's equations reduce to uncoupled wave equations:

$$\frac{1}{c^2}\frac{\partial^2 \Phi}{\partial t^2} - \Delta \Phi = \rho/\varepsilon_0$$
$$\frac{1}{c^2}\frac{\partial^2 \mathbf{A}}{\partial t^2} - \Delta \mathbf{A} = \mu_0 \mathbf{J}$$

with $\mathbf{E} = -\nabla\Phi - \frac{\partial \mathbf{A}}{\partial t}$ and $\mathbf{B} = \nabla \times \mathbf{A}$ [21].

In the electromagnetic case, we will solve these wave equations coupled into a particle-in-cell method to constitute a solution of the usual Vlasov-Maxwell system. In the non-relativistic, zero-magnetic field limit, we drop $\mathbf{A}$ and the corresponding wave equations and consider a quasi-electrostatic Vlasov-Wave model, which will agree with the electrostatic Vlasov-Poisson model when $|\mathbf{v}|/c << 1$. This condition frequently can be interpreted as $\omega_p L << c$ for a relevant physical length scale L, where ω_p is the (electron) plasma frequency. The resulting Vlasov-Wave system is as follows:

$$\frac{\partial f}{\partial t} + \mathbf{v} \cdot \nabla_{\mathbf{x}} f - \frac{q}{m} \nabla \Phi \cdot \nabla_{\mathbf{v}} f = 0$$
$$\frac{1}{c^2}\frac{\partial^2 \Phi}{\partial t^2} - \Delta \Phi = \rho/\varepsilon_0, \quad \rho(\mathbf{x}, t) = q \int_{\mathbf{v}} f(\mathbf{x}, \mathbf{v}, t) d\mathbf{v}$$

The purpose of this work is the numerical solution of (nondimensionalized forms of) these systems with PIC methods that avoid imposing a CFL stablity restriction related to the speed of light due to the presence of the wave equations for Φ and $\mathbf{A}$.

3. Wave Solver Description

3.1. **Origin and Mitigation of the CFL Restriction.** Consider the Cauchy problem for the wave equation:

$$u_{tt} = c^2 \Delta u \tag{1}$$
$$u(x, 0) = g(x) \tag{2}$$
$$u_t(x, 0) = h(x). \tag{3}$$

To see the origin of the CFL restriction in a typical explicit finite difference method, consider the semi-discrete scheme obtained by substituting the centered, second-order finite difference discretization of u_{tt} into the wave equation. We obtain

$$\frac{u(x, t + \Delta t) - 2u(x, t) + u(x, t - \Delta t)}{\Delta t^2} = c^2 \Delta^2 u(x, t).$$

Upon Fourier transforming in the spatial variable, we obtain

$$\hat{u}(\xi, t + \Delta t) - 2\hat{u}(\xi, t) + \hat{u}(\xi, t - \Delta t) = -c^2 \Delta t^2 |\xi|^2 \hat{u}(\xi, t) \tag{4}$$

where ξ is the spatial frequency. The problem is that a high-frequency perturbation of u - such as that introduced by truncation error - will be amplified by the symbol $-c^2 \Delta t^2 |\xi|^2$, resulting in instability. In a fully discrete method, the spatial frequencies are bounded by $2/\Delta x$ (the Nyquist frequency), meaning that $c\Delta t/\Delta x$ must be sufficiently small to prevent

amplification of high frequencies. In terms of semi-discrete Von Neumann analysis, consider substituting into 4 a semi-discrete solution of the form $\hat{u}(\xi, n\Delta t) = \lambda^n$ for some $\lambda \in \mathbb{C}$. We obtain a quadratic equation $\lambda^2 - (2 - z^2)\lambda + 1 = 0$ and the stability condition $|\lambda| \leq 1$ for any root λ of this equation, where $z = c\Delta t|\xi|$. It is easily verified from the quadratic formula that the roots λ_i satisfy $|\lambda_i| \leq 1$ for $i = 1, 2$ if and only if $|z| \leq 2$, that is if and only if $c\Delta t \leq 2/|\xi|$. For the 1D case, inserting the Nyquist frequency $2/\Delta x$ into the upper bound gives the usual CFL stability restriction $c\Delta t \leq \Delta x$.

To avoid the CFL restriction while maintaining an explicit update equation, we modify the symbol of the Laplacian to bound it and prevent the amplification of high frequencies. Consider the one-dimensional case. We look for bounded rational approximations of ξ^2 near $\xi = 0$. One option is

$$\xi^2 \approx \frac{\alpha^2\xi^2}{\xi^2 + \alpha^2} \approx \xi^2(1 - (\xi/\alpha)^2 + \cdots)$$

We can write this modified semi-discrete scheme in Fourier space as

$$\hat{u}(\xi, t + \Delta t) - 2\hat{u}(\xi, t) + \hat{u}(\xi, t - \Delta t) = -c^2\Delta t^2 \frac{\alpha^2\xi^2}{\xi^2 + \alpha^2}\hat{u}(\xi, t)$$

Choosing $\alpha = \beta/c\Delta t$ for some properly chosen β, we can see that the modified symbol is uniformly bounded by β^2 for all Δt, so that choosing $\beta \leq 2$ will ensure stability, independently of Δt, and it turns out that $\beta = 2$ gives optimal accuracy for stable schemes of this family [7, 9]. Multiplication in Fourier space is equivalent to convolution in physical space, so transforming back into physical space gives a method based on convolution with the inverse Fourier transform of the modified symbol:

$$u(x, t + \Delta t) - 2u(x, t) + u(x, t - \Delta t) = -\beta^2 D[u](x, t)$$

where $D[f](x) = \int(\delta(x - x') - \frac{\alpha}{2}e^{-\alpha|x-x'|})f(x')\,dx' = f(x) - \int \frac{\alpha}{2}e^{-\alpha|x-x'|}f(x')\,dx'$.

As a general comment, this modification of the symbol of the Laplacian introduces error at high spatial frequencies, so that this technique may not be suitable for problems in which extremely accurate propagation of waves at high spatial frequencies (high wavenumber) is essential. However, in many problems of plasma physics, the physics is dominated by effects at low spatial frequencies, and in these problems this technique can find useful application.

A detailed discussion of numerical methods for the wave equation derived from the perspective of Fourier multipliers, including higher-order methods and the extension to multiple dimensions, can be found in [9]. In the following section, we give the derivation of two useful second-order numerical methods through alternative means, the Method of Lines Transpose, which also facilitates the extension of the methods to bounded domains and to multiple dimensions.

3.2. **Method of Lines Transpose: Derivation of Semi-Discrete Schemes.** In the Method of Lines Transpose for the solution of time-dependent PDEs, also known as Rothe's method [33], finite difference discretizations of time derivatives are substituted into the PDE, resulting in a boundary value problem (BVP) to be solved at each time step. In recent years, the MOLT has been applied as a numerical method to solve various time-dependent PDEs, with initial focus on parabolic equations [10, 19, 20, 6, 25]. The work [8] extended this

approach to the second order wave equation, and is the basis of the present work. Further work extended this approach to higher dimensions through dimensional splitting [7] and to higher-order through the Fourier multiplier approach mentioned in the previous section [9]. Based on the work in [8, 7, 9], we give here an overview of the derivation of two useful second-order schemes for the wave equation, their extension to multiple dimensions through dimensional splitting, and a fast numerical algorithm for the 1D problem. In Section 7, we give semi-discrete Von Neumann analyses and dispersion relations for these semi-discrete schemes, along with a new proof that the fully discrete versions are unconditionally stable, in the sense of Von Neumann analysis.

3.2.1. *Dispersive Semi-Discrete Scheme.* As in the previous section, we substitute the following second-order centered discretization into the wave equation $\frac{1}{c^2}u_{tt} - \Delta u = f(x,t)$:

$$u_{tt}^n = \frac{u^{n+1} - 2u^n + u^{n-1}}{\Delta t^2} - \frac{\Delta t^2}{12} u_{tttt}(x,\eta).$$

Instead of proceding by the Fourier multiplier approach as mentioned previously, we apply an averaging technique with similar results. We average the Laplacian term in time

$$\Delta u^n = \frac{1}{4}\Delta\left(u^{n+1} + 2u^n + u^{n-1}\right) + O(\Delta t^2)$$

and substitute into the wave equation. Defining $\alpha = 2/(c\Delta t)$ and manipulating gives the semi-discrete scheme

$$\left(-\frac{1}{\alpha^2}\Delta + 1\right)\left(u^{n+1} + 2u^n + u^{n-1}\right) = 4u^n + \frac{4}{\alpha^2} f(x,t^n) + O(\Delta t^4).$$

We call this the dispersive semi-discrete scheme, since all terms in the semi-discrete dispersion relation are real-valued (see 7.2).

3.2.2. *Diffusive Semi-Discrete Scheme.* We substitute the following backward difference formula (BDF) discretization:

$$u_{tt}^{n+1} = \frac{2u^{n+1} - 5u^n + 4u^{n-1} - u^{n-2}}{\Delta t^2} - \frac{11\Delta t^2}{12} u_{tttt}(x,\eta)$$

into the wave equation $\frac{1}{c^2}u_{tt} - \Delta u = f(x,t)$.

Rearranging, defining $\alpha = \sqrt{2}/(c\Delta t)$ and dividing by α^2 gives the semi-discrete scheme

$$\left(-\frac{1}{\alpha^2}\Delta + 1\right) u^{n+1} = \frac{1}{2}\left(5u^n - 4u^{n-1} + u^{n-2}\right) + \frac{1}{\alpha^2} f(x,t^{n+1}) + O(\Delta t^4).$$

We call this the diffusive semi-discrete scheme, due to the presence of imaginary-valued terms in the semi-discrete dispersion relation (see 7.2). The (slight) dissipation of this method proved useful in our PIC simulations, and we use this scheme (rather than the dispersive scheme) in all numerical test problems in this work.

3.3. **Solution of the Modified Helmholtz Equation.** As seen in the previous section, both the dispersive and diffusive semi-discrete schemes include an elliptic BVP to be solved at each time step. The resulting PDE is sometimes called the modified Helmholtz equation [20]. In contrast to the usual frequency-domain Helmholtz equation $\Delta u + \frac{\omega^2}{c^2} u = f$, the modified Helmholz equation has a nonoscillatory Green's function. The oscillation in the solution of the wave equation is supported by the presence of multiple time levels in the semi-discrete equations. Our solution strategy is to use the well-known technique of dimensional splitting [29] to reduce problems in multiple dimensions to problems in one dimension, to which we apply a fast integral solution method. The dimensionally-split integral solution naturally leads to unconditionally stable numerical schemes with computational cost and coding complexity comparable to explicit schemes.

3.3.1. *Dimensional Splitting.* For smooth $u(x, y)$, we have

$$\left(-\frac{1}{\alpha^2}\left(\partial_{xx} + \partial_{yy}\right) + 1\right) u = \left(-\frac{1}{\alpha^2}\partial_{xx} + 1\right)\left(-\frac{1}{\alpha^2}\partial_{yy} + 1\right) u - \frac{1}{\alpha^4}\partial_{xxyy} u$$

So, to approximately solve $\left(-\frac{1}{\alpha^2}\left(\partial_{xx} + \partial_{yy}\right) + 1\right) u = f$ we will instead solve

$$\left(-\frac{1}{\alpha^2}\partial_{xx} + 1\right)\left(-\frac{1}{\alpha^2}\partial_{yy} + 1\right) u = f.$$

where we have introduced the splitting error

$$\frac{1}{\alpha^4}\partial_{xxyy} u = O(c^4 \Delta t^4).$$

To solve

$$\left(-\frac{1}{\alpha^2}\partial_{xx} + 1\right)\left(-\frac{1}{\alpha^2}\partial_{yy} + 1\right) u = f$$

we define $w = \left(-\frac{1}{\alpha^2}\partial_{yy} + 1\right) u$ and solve the following one-dimensional BVPs "line by line":

$$\left(-\frac{1}{\alpha^2}\partial_{xx} + 1\right) w(x, \cdot) = f(x, \cdot)$$
$$\left(-\frac{1}{\alpha^2}\partial_{yy} + 1\right) u(\cdot, y) = w(\cdot, y)$$

where appropriate boundary conditions are supplied (see [8, 9]). To facilitate the "line-by-line" solution, we discretize the domain with a uniform Cartesian grid.

3.3.2. *Integral Solution Method in 1D.* Consider the modified Helmholtz equation in one dimension, $\left(-\frac{1}{\alpha^2}\frac{d^2}{dx^2} + 1\right) u = f(x)$ for $x \in \Omega = (a, b)$, with appropriate boundary conditions imposed at $x = a$ and $x = b$. We can write $u(x) = u^P(x) + u^H(x)$, where

$$u^P(x) = \frac{\alpha}{2}\int_a^b f(x') e^{-\alpha|x - x'|}\, dx'$$
$$u^H(x) = A e^{-\alpha(x-a)} + B e^{-\alpha(b-x)}$$

are the particular and homogeneous solutions and where A and B depend on the boundary conditions imposed, as well as the values of $u^P(a)$ and $u^P(b)$ [8]. Our fast integral solver consists of a fast convolution algorithm for the evaluation of the particular solution u^P,

along with appropriate algorithms for evaluating the homogeneous solution u^H, which can be viewed as boundary correction terms. For many common boundary conditions, the coefficients A and B for the boundary correction terms can be found by applying the given boundary conditions and solving a 2×2 system by hand for A and B. For instance, in the case of homogeneous Dirichlet boundary conditions $u(a) = u(b) = 0$ and defining $\gamma = e^{-\alpha(b-a)}$, we find

$$A = \frac{\gamma u^P(b) - u^P(a)}{1-\gamma^2}$$
$$B = \frac{\gamma u^P(a) - u^P(b)}{1-\gamma^2}.$$

In the case of periodic boundary conditions, we find

$$A = \frac{u^P(b)}{1-\gamma}$$
$$B = \frac{u^P(a)}{1-\gamma}.$$

With some further consideration, other boundary conditions can be derived, including outflow (absorbing) boundary conditions (for the underlying wave equation, based on one-way wave equations). For further details, see [8, 7, 9].

3.3.3. *Fast Numerical Evaluation of the 1D Convolution Operator.* The convolution operator giving the particular solution can be decomposed as

$$\begin{aligned} I[f](x) &= \frac{\alpha}{2}\int_{-\infty}^{\infty} f(x')e^{-\alpha|x-x'|}\,dx' \\ &= \frac{\alpha}{2}\int_{-\infty}^{x} f(x')e^{-\alpha|x-x'|}\,dx' + \frac{\alpha}{2}\int_{x}^{\infty} f(x')e^{-\alpha|x-x'|}\,dx' \\ &=: I^L[f](x) + I^R[f](x) \end{aligned}$$

for a given function f. Meanwhile, we have the recursion relations

$$I^L[f](x) = e^{-\alpha\Delta x}I^L[f](x-\Delta x) + \frac{\alpha}{2}\int_{x-\Delta x}^{x} f(x')e^{-\alpha(x-x')}\,dx'$$
$$I^R[f](x) = e^{-\alpha\Delta x}I^R[f](x+\Delta x) + \frac{\alpha}{2}\int_{x}^{x+\Delta x} f(x')e^{-\alpha(x'-x)}\,dx'.$$

Based on these observations, we outline the fast algorithm for the numerical evaluation of this convolution operator on a uniform Cartesian grid developed in [8, 7, 9]. Consider the convolution operator applied to a function f supported on the interval (a, b), with the convolution also to be evaluated in (a, b). The interval is discretized into N equal subintervals of length $\Delta x = (b-a)/N$, with endpoints $x_1 = a$, $x_{j+1} = x_j + \Delta x$ for $j = 1, ..., N$. We denote $I_j = I[f](x_j)$, $I_j^L = I^L[f](x_j)$ and $I_j^R = I^R[f](x_j)$, as defined above. Further, we define the

local integrals

$$J_j^L = \frac{\alpha}{2}\int_{x_{j-1}}^{x_j} f(x')e^{-\alpha(x_j-x')}\,dx' \quad j = 2, ..., N+1$$
$$J_j^R = \frac{\alpha}{2}\int_{x_j}^{x_{j+1}} f(x')e^{-\alpha(x'-x_j)}\,dx' \quad j = 1, ..., N.$$

Suppose we have already computed these J_j^L and J_j^R. Setting $I_1^L = I_{N+1}^R = 0$, we can then perform a recursive evaluation of the convolution integral by computing $I_{j+1}^L = e^{-\alpha\Delta x} I_j^L + J_{j+1}^L$ and $I_{N+1-j}^R = e^{-\alpha\Delta x} I_{N+1-j+1}^R + J_{N+1-j}^R$ for $j = 1, ...N$. We then sum $I_j = I_j^L + I_j^R$ for each $j = 1, ..N+1$.

The method for evaluating the local integrals J_j^L and J_j^R depends on the nature of the integrand. For the particle convolution integral, where the integrand is the sum of particle shape functions, we can analytically evaluate the local integrals. This is described in Section 4. For general integrands, and specifically for the terms involving u on the right hand sides of the semi-discrete schemes, we numerically evaluate the local integrals with a quadrature rule. It is important to note that any given quadrature rule may or may not deliver an accurate and stable overall scheme for the wave equation. To achieve accuracy and stability, we use a quadrature rule found by analytically integrating against a Lagrange polynomial interpolant. For a quadratic interpolant, leading to second-order accurate quadrature in space, we obtain the following approximations

$$J_j^L \approx Pf(x_j) + Qf(x_{j-1}) + R(f(x_{j+1}) - 2f(x_j) + f(x_{j-1}))$$
$$J_j^R \approx Pf(x_j) + Qf(x_{j+1}) + R(f(x_{j+1}) - 2f(x_j) + f(x_{j-1}))$$

where, defining $\nu = \alpha\Delta x$ and $d = e^{-\nu}$,

$$P = 1 - \frac{1-d}{\nu}$$
$$Q = -d + \frac{1-d}{\nu}$$
$$R = \frac{1-d}{\nu^2} - \frac{1+d}{2\nu}$$

Higher-order spatial accuracy can be obtained by using higher-order accuracy quadrature rules, with the outcome of unconditional stability limiting the choice of quadrature rules. Further details can be found in [8, 7, 9]. In the Appendix, Von Neumann analyses are carried out for the fully discrete diffuse and dispersive schemes in one and multiple dimensions, and it is shown that they are both unconditionally stable.

4. Implementation of Particles

4.1. **Particle Weighting Scheme.** In our PIC methods, the charge and current densities are represented as the sum of particle shape functions:

$$\rho(\mathbf{x},t) = \sum_{i=1}^{N_p} q_i S\left(\frac{\mathbf{x}-\mathbf{x}_{p,i}(t)}{\Delta x}\right)$$
$$\mathbf{J}(\mathbf{x},t) = \sum_{i=1}^{N_p} q_i \mathbf{v}_{p,i} S\left(\frac{\mathbf{x}-\mathbf{x}_{p,i}(t)}{\Delta x}\right)$$

where N_p is the number of particles, $\mathbf{x}_{p,i}(t)$ and $\mathbf{v}_{p,i}(t)$ are the position and velocity, respectively, of particle i at time t, and $S(\mathbf{x})$ is a particle shape function. It should be emphasized that these are not physical particles, but rather macro- or superparticles that represent a discretization of the PDF [4]. We do not directly weight particle charge and current density to the grid, but rather we analytically evaluate the particle convolution integrals corresponding to these source terms with the algorithm described below.

4.2. **Method for Controlling Divergence Error.** It is well known that electromagnetic PIC methods which do not satisfy a discrete form of Gauss' law through their field solvers and charge and current weighting schemes will suffer severe numerical errors related to charge conservation [26]. We seek to develop staggered grid approaches to computing potentials and fields that satisfy discrete analogues of Gauss' law $\nabla \cdot \mathbf{E} = \rho/\epsilon_0$ and the identity $\nabla \cdot \mathbf{B} = 0$. The divergence-free condition for $\mathbf{B}$ will be easily satisfied in general, as the magnetic field will be calculated as a finite difference curl of the vector potential. In order to numerically enforce Gauss' law, we seek to perform an elliptic divergence correction. Future work will consider the alternative of hyperbolic divergence cleaning.

We now give the mathematical underpinning of our elliptic divergence correction technique. The electric field is calculated as $\mathbf{E} = -\nabla\Phi - \frac{\partial \mathbf{A}}{\partial t}$. Then Gauss' law may be rewritten as:

$$\begin{aligned}\rho/\epsilon_0 &= \nabla \cdot \mathbf{E} \\ &= \nabla \cdot (-\nabla\Phi - \frac{\partial \mathbf{A}}{\partial t}) \\ &= -\Delta\Phi - \frac{\partial (\nabla \cdot \mathbf{A})}{\partial t}.\end{aligned}$$

Thus, the scalar potential satisfies the Poisson equation

$$-\Delta\Phi = \rho/\epsilon_0 + \frac{\partial (\nabla \cdot \mathbf{A})}{\partial t}$$

Our method is based on the observation that if this Poisson equation is suitably discretized and solved on a staggered grid to provide the scalar potential used in calculating the electric field, then the electric field will automatically satisfy a discrete form of Gauss' law. While the exact form of the staggered grid will depend on which components of the current density and the electric and magnetic fields are retained in a given model, our method guarantees exact discrete divergence relations independently of the charge and current weighting schemes used, of the nature of the solver used for $\mathbf{A}$, and of the gauge condition specified.

4.3. **Particle Equations of Motion.** In our PIC methods, the approximation of the evolution of the Vlasov equation amounts to the integration of the equations of motion of the particles:

$$\frac{d\mathbf{x}_{p,i}}{dt} = \mathbf{v}_{p,i}(t)$$
$$\frac{d\mathbf{v}_{p,i}}{dt} = \mathbf{a}_{p,i}(t)$$

where $\mathbf{a}_{p,i}(t)$ is the acceleration of particle i at time t. To evolve the particle equations of motion, we use standard numerical methods, such as the explicit leapfrog method, and obtain particle accelerations through the usual interpolation of fields from grid points to particle locations [4]. Fields are calculated as finite differences of potentials on the grid. As these aspects are standard and not the focus of the present work, we do not elaborate further.

4.4. **Fast Convolution Algorithm in 1D.** We now describe the algorithm used for the fast exact evaluation of the convolution of charge and current density source terms due to particles. It has two main steps. There is a local deposit step and then a recursive sweep step. This basic structure is the same in all dimensions. For definiteness, we describe the application of the algorithm to linear particle shapes in one and two dimensions. However, it may be generalized to any separable particle shapes with compact support in any dimension. Note that this includes many widely used particle shapes in PIC algorithms, namely typical spline-based particle shapes and (suitably cut-off) Gaussian particle shapes. For the case of the charge density integral, the particle shape function S_p below is replaced by $q_p S_p$ and its contribution summed to the charge density integral, and for the case of the current density integral, S_p is replaced by $\mathbf{v}_p q_p S_p$ and its contribution summed to the current density integral.

4.4.1. *Local Deposit Step in 1D.* Consider particle p located in the cell $[x_m, x_{m+1}]$ in a uniform grid with cell length Δx. Let $S_p(x)$ be the shape function of the particle. Assume that the support of S_p has length $2r\Delta x$ for some integer r. The local deposit step then consists of analytically evaluating the integrals

$$J_{j+1}^{L,p} = \alpha \int_{x_j}^{x_{j+1}} S_p(x') e^{-\alpha(x_{j+1}-x')}\, dx'$$
$$J_{j}^{R,p} = \alpha \int_{x_j}^{x_{j+1}} S_p(x') e^{-\alpha(x'-x_j)}\, dx'$$

for $j = m - r, ..., m, ..., m + r$ and for each particle p, and summing their values on the grid.

For linear particle shapes (corresponding to $r = 1$), we have $S_p(x) = S(\frac{x-x_p}{\Delta x})$, where

$$S(x) = \begin{cases} 1 - |x| & |x| < 1, \\ 0 & |x| \geq 1 \end{cases}$$

Let $a = (x_p - x_m)/\Delta x$, where x_p is the location of the particle. For simplicity, let $x_p = 0$ and $\Delta x = 1$. For linear particle shapes, we then have the situation displayed in Figure 1.

The desired integrals are then easily evaluated for linear particle shapes:

$$
\begin{aligned}
J_m^{L,p} &= \alpha \int_{-1}^{-a} (1+x')e^{-\alpha(-a-x')}\,dx' \\
&= (((1-a)\alpha - 1) + e^{\alpha a}e^{-\alpha})/\alpha \\
J_{m+1}^{L,p} &= \alpha \int_{-a}^{1-a} (1-|x'|)e^{-\alpha(1-a-x')}\,dx' \\
&= (e^{-\alpha}((a-1)\alpha + 1) + a\alpha + 1 - 2e^{-\alpha}e^{\alpha a})/\alpha \\
J_{m+2}^{L,p} &= \alpha \int_{1-a}^{1} (1-x')e^{-\alpha(2-a-x')}\,dx' \\
&= (e^{-\alpha}(-a\alpha - 1) + e^{-\alpha}e^{\alpha a})/\alpha \\
J_{m-1}^{R,p} &= \alpha \int_{-1}^{-a} (1+x')e^{-\alpha(x'-(-1-a)}\,dx' \\
&= (e^{-\alpha}((a-1)\alpha - 1) + e^{-\alpha a})/\alpha \\
J_m^{R,p} &= \alpha \int_{-a}^{1-a} (1-|x'|)e^{-\alpha(x'-(-a)}\,dx' \\
&= ((1-a)\alpha + 1 + e^{-\alpha}(-a\alpha + 1) - 2e^{-\alpha a})/\alpha \\
J_{m+1}^{R,p} &= \alpha \int_{1-a}^{1} (1-x')e^{-\alpha(x'-(1-a))}\,dx' \\
&= (a\alpha - 1 + e^{-\alpha a})/\alpha
\end{aligned}
$$

Note that just one evaluation of an exponential function is required per particle (namely $e^{\alpha a}$). To account for arbitrary Δx, we make the substitution $\alpha \leftarrow \alpha\Delta x = \nu$.

To obtain the total local deposit, we simply sum the particle contributions on to the grid. Let N_p be the total number of particles. The algorithm for the local deposit step is given by:

Initialize $J_k^L = J_k^R = 0$ for all k.
for $p = 1 : N_p$ **do**
Particle p located in cell $[x_m, x_{m+1}]$.

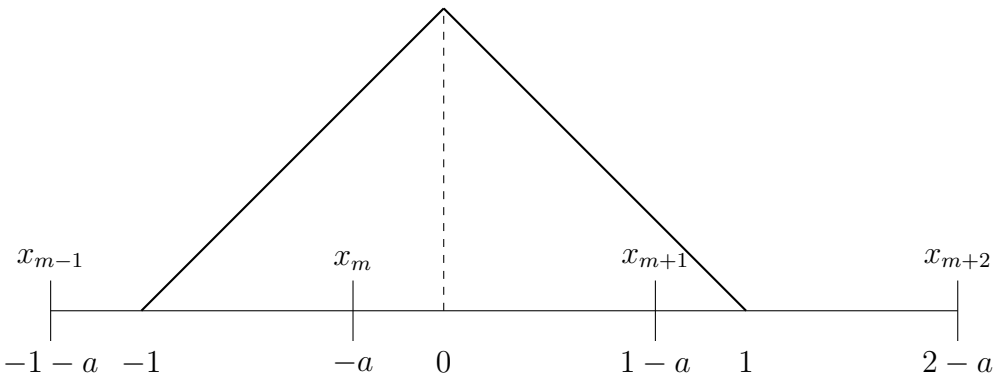

FIGURE 1. $S(x) = 1 - |x|, |x| < 1, S(x) = 0, |x| \geq 1$

for $j = m - r : m + r$ **do**
Compute $J^{L,p}_{j+1}$, $J^{R,p}_j$
Deposit $J^L_{j+1} = J^L_{j+1} + J^{L,p}_{j+1}$, $J^R_j = J^R_j + J^{R,p}_j$
end for
end for

Note that the local deposit step costs $O(N_p)$ operations.

4.4.2. *Recursive Sweep Step in 1D.* Once we have performed the local deposit step, we complete the evaluation of the particle integral with a recursive sweep step. Suppose we have N gridpoints, $x_1, ..., x_N$. The algorithm for the recursive sweep step is given by:

Initialize $I^L_1 = I^R_N = 0$
for $j = 1 : N - 1$ **do**
$I^L_{j+1} = J^L_{j+1} + e^{-\nu} I^L_j$
$I^R_{N-j} = J^R_{N-j} + e^{-\nu} I^R_{N-j+1}$
end for
$I = I^L + I^R$

Note that the recursive sweep step costs $O(N)$ operations.

4.5. **Fast Convolution Algorithm in 2D.** For a separable particle shape $S(x, y) = S_x(x)S_y(y)$, we have

$$\begin{aligned} I_x[I_y[S]](x,y) &= I_x[S_x](x) \cdot I_y[S_y](y) \\ &= \big(I^L_x[S_x](x) + I^R_x[S_x](x)\big) \cdot \big(I^D_y[S_y](y) + I^U_y[S_y](y)\big) \\ &= I^L_x[S_x](x) \cdot I^D_y[S_y](y) + I^L_x[S_x](x) \cdot I^U_y[S_y](y) + \\ &\quad + I^R_x[S_x](x) \cdot I^D_y[S_y](y) + I^R_x[S_x](x) \cdot I^U_y[S_y](y) \end{aligned}$$

This is suggestive of how we will build the 2D algorithm.

4.5.1. *Local Deposit Step in 2D.* Consider particle p centered at $(x_p, y_p) \in [x_m, x_{m+1}] \times [y_n, y_{n+1}]$, with separable particle shape $S_p(x, y) = S(\frac{x-x_p}{\Delta x})S(\frac{y-y_p}{\Delta y})$ where

$$S(x) = \begin{cases} 1 - |x| & |x| < 1, \\ 0 & |x| \geq 1 \end{cases}$$

The support of the particle shape is shown in Figure 2.

In the local deposit step, we form a tensor product on the grid as suggested by the above decomposition. Note that a total of 12 local integrals must be evaluated for each particle, then summed onto the grid as a tensor product.

Initialize $J^{LU}_{j,k} = J^{LD}_{j,k} = J^{RU}_{j,k} = J^{RD}_{j,k} = 0$ for all j, k.
for $p = 1 : N_p$ **do**
Particle p located in cell $[x_m, x_{m+1}] \times [y_n, y_{n+1}]$.
for $j = m - r : m + r$, $k = n - r : n + r$ **do**
Compute $J^{L,p}_{j+1}$, $J^{R,p}_j$, $J^{D,p}_{k+1}$, $J^{U,p}_k$
Deposit:
$J^{LD}_{j+1,k+1} = J^{LD}_{j+1,k+1} + J^{L,p}_{j+1} \cdot J^{D,p}_{k+1}$
$J^{LU}_{j+1,k} = J^{LU}_{j+1,k} + J^{L,p}_{j+1} \cdot J^{U,p}_k$

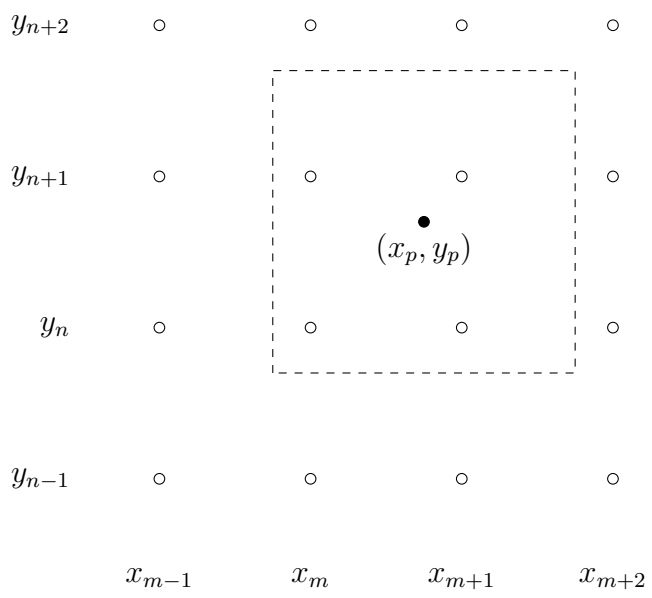

FIGURE 2. The support of a linear particle shape $Sp(x, y)$ in 2D.

$J^{RD}_{j,k+1} = J^{RD}_{j,k+1} + J^{R,p}_j \cdot J^{D,p}_{k+1}$
$J^{RU}_{j,k} = J^{RU}_{j,k} + J^{R,p}_j \cdot J^{U,p}_k$
end for
end for

4.5.2. *Recursive Sweep Step in 2D.* The recursive sweep step is similar to the 1D case, and is given below.

for $k = 1 : N_y$ **do**
Initialize $I^{LD}_{1,k} = I^{LU}_{1,k} = I^{RD}_{N_x,k} = I^{RU}_{N_x,k} = 0$.
for $j = 1 : N_x - 1$ **do**
$I^{LD}_{j+1,k} = J^{LD}_{j+1,k} + e^{-\nu} I^{LD}_{j,k}$
$I^{LU}_{j+1,k} = J^{LU}_{j+1,k} + e^{-\nu} I^{LU}_{j,k}$
$I^{RD}_{N_x-j,k} = J^{RD}_{N_x-j,k} + e^{-\nu} I^{RD}_{N_x-j+1,k}$
$I^{RU}_{N_x-j,k} = J^{RU}_{N_x-j,k} + e^{-\nu} I^{RU}_{N_x-j+1,k}$
end for
end for
$J^D = I^{LD} + I^{RD}$
$J^U = I^{LU} + I^{RU}$
for $j = 1 : N_x$ **do**
Initialize $I^D_{j,1} = I^U_{j,N_y} = 0$.
for $k = 1 : N_y - 1$ **do**
$I^D_{j,k+1} = J^D_{j,k+1} + e^{-\nu} I^D_{j,k}$
$I^U_{j,N_y-k} = J^U_{j,N_y-k} + e^{-\nu} I^U_{j,N_y-k+1}$
end for
end for
$I = I^D + I^U$

Both 1D and 2D overall algorithms cost $O(N_p + N)$ operations, where N is the total number of gridpoints. Since in a typical PIC simulation, $N_p >> N$, the cost of the overall algorithm is dominated by the local deposit step.

4.6. **Particle Boundary Conditions.** In dealing with boundaries, two types of considerations must be made. First, we must determine what to do in the integration of boundary particles, for which the support of the shape function extends outside of the domain. This will be dependent upon the type of boundary condition. For periodic boundary conditions, we can simply extend the particle shape function periodically and proceed to integrate. For Dirichlet boundary conditions, we extend the integration domain to include ghost points just beyond the boundary to which the boundary particles are weighted.

Second, we must ensure that the particle convolution integral is consistent with the boundary conditions on the wave function. This is easily handled through the usual boundary correction terms in one-dimension, and can be extended to the dimensionally-split multidimensional case.

5. Numerical Results

5.1. **Electrostatic Test Problems.** We first consider three standard periodic electrostatic test problems in 1D and 2D, then a 1D bounded plasma problem, the simulation of sheath formation. In the first three test problems, electrons are loaded from a perturbed initial distribution of the form

$$f_e(x, v, t = 0) = f_e(v)\left(1 + \epsilon \sin\left(\frac{2\pi x}{L_x}\right)\right) \tag{5}$$

where L_x is the length of the domain, ϵ is the amplitude of perturbation, and $f_e(v)$ is the initial velocity distribution. In the 2D case, simulations are taken to be uniform in the y-direction. We normalize quantities according to the nondimensionalization presented in the Section 7.1.1. In particular, we normalize time quantities to the inverse plasma frequency ω_p^{-1}. We will consider a periodic domain with a uniform neutralizing background charge, and further we set the speed of light $c = 100$. In these problems, we see good performance even at large CFLs, since the physics is dominated by the low frequency spatial modes.

5.1.1. *Cold Plasma Langmuir Wave.* We consider a cold plasma Langmuir wave [4] with $f_e(v) = \delta(v)$. Electrons are perturbed away from a uniformly distributed, motionless state against a static, uniform neutralizing background charge distribution. The resulting separation of charge produces cold plasma oscillation. In the 1D simulation, we set $L_x = 2\pi$ and $\epsilon = 0.1$. We use a 100 cell grid and take $\Delta t = 0.1$, and we use $N_p = 3600$ particles. In the 2D simulation, we set $L_x = L_y = 2\pi$ and the perturbation strength $\epsilon = 0.1$. We use a 100×100 grid and again take $\Delta t = 0.1$, and we use $N_p = 360000$ particles. In both 1D and 2D cases, the CFL number used is $c\Delta t/\Delta x \approx 159$, much larger than what would be allowed by an explicit method. The oscillation in the potential energy is plotted and compared to the prediction of linear theory in Figure 3; we see that the plasma frequency is accurately reproduced.

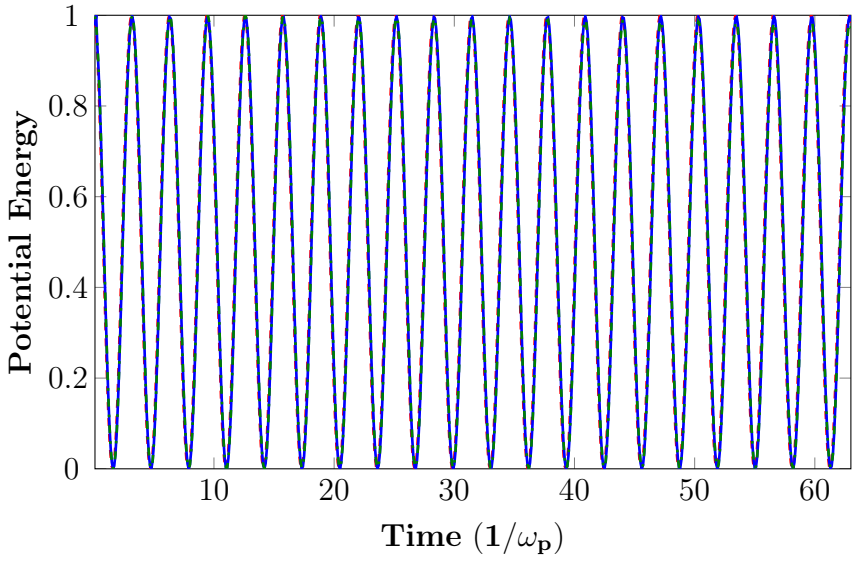

FIGURE 3. Potential energy in cold plasma oscillation. Green is the 1D numerical result, blue is the 2D numerical result, and red is the prediction of linear theory. We see the plasma frequency is accurately reproduced in our simulations.

5.1.2. *Two Stream Instability.* We consider the two stream instability with $f_e(v) = \delta(v - v_{\text{beam}}) + \delta(v + v_{\text{beam}})$. Two counterstreaming beams of electrons are perturbed away from a uniformly distributed state against a static, uniform neutralizing background charge distribution. The beams interact and "roll up" in phase space, causing some of the particles' kinetic energy to be transformed into potential energy stored in the electric field. According to the dispersion relation for the two stream instability from linear theory [4], we have

$$\omega^4 - 2\omega^2(\omega_p^2 + k^2 v_{\text{beam}}^2) + k^2 v_{\text{beam}}^2(k^2 v_{\text{beam}}^2 - 2\omega_p^2) = 0 \tag{6}$$

which gives the greatest growth rate, $\gamma \approx 0.3535$, for $k \approx 3.06$. We therefore scale the domain to this value of k, and take $L_x = 2\pi/3.06$. We take the beam velocity $v_{\text{beam}} = 1$ and the perturbation strength $\epsilon = 0.0005$. In our 1D simulation, we use a 100 cell grid with $\Delta t = 0.1$, and we use $N_p = 1000$ particles. In our 2D simulation, we use a 100×100 grid with $\Delta t = 0.1$, and we use $N_p = 1000000$ particles. This results in a CFL number of $c\Delta t/\Delta x \approx 68$. We run the simulations for 1000 time steps. The growth of the $k = 3.06$ mode of the electric field is shown in Figure 4 for the 1D and 2D cases, and agrees with the rate from linear theory. In the nonlinear saturation stage, we see a slight discrepancy between the 1D and 2D results, probably due to the accumulation of numerical error. We also show selected phase space plots in Figure 5, where we see the expected "rolling up" of the two beams. Resolution is limited by the number of particles.

5.1.3. *Landau Damping.* We consider Landau damping of Langmuir waves in a warm plasma, with $f_e(v)$ taken to be Maxwellian. Warm electrons, following a Maxwellian velocity distribution, are perturbed away from a unifom distribution against a static, uniform neutralizing background charge distribution. Potential energy from the electric field is transformed into kinetic energy of particles. The dispersion relation from linear theory in this case gives a

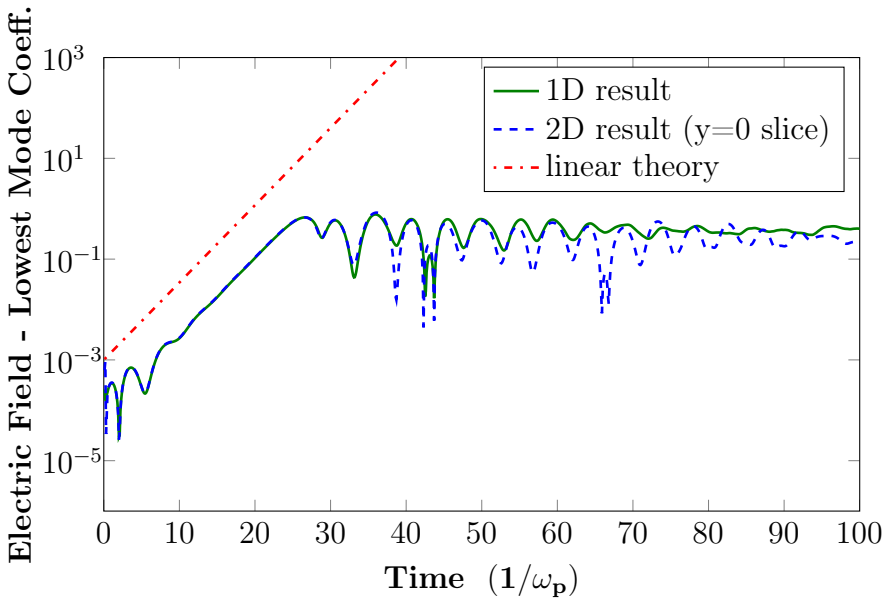

FIGURE 4. Growth of the mode with maximum growth rate in the two stream instability, corresponding to $k = 3.06$. Green is the 1D numerical result, blue is the 2D numerical result (measured along the central $y = 0$ slice), and red is the prediction of linear theory. We see the correct growth rate is reproduced in our simulations.

decay rate of $\gamma \approx 0.154$ for the $k = 0.5$ mode [4]. We take $L_x = 4\pi$, electron thermal velocity $v_{\text{therm}} = 1$ and perturbation strength $\epsilon = 0.1$. In our 1D simulation, we use a 100 cell grid and take $\Delta t = 0.1$, and we use $N_p = 1000000$ particles. In our 2D simulation, we use a 100×100 grid and take $\Delta t = 0.1$, and we use $N_p = 9000000$ particles. We run the simulations for 300 time steps. The decay of the $k = 0.5$ mode of the electric field in the 1D and 2D simulations is shown in Figure 6, and agrees with the rate from linear theory. As in the two stream instability example, there is a discrepancy between the 1D and 2D results at later times, again likely due to the accumulation of numerical errors.

5.1.4. *Sheath Formation in a Bounded 1D Plasma.* We present the simulation of sheath formation in a bounded 1D plasma, following the model described in [32]. In contrast to the previous problems, this simulation incorporates both mobile electrons and ions. Electrons and ions are initialized from Maxwellian distributions and uniformly spatially distributed in a bounded domain. The left boundary is a symmetry plane, and so we impose Neumann boundary conditions on the potential, and reflux boundary conditions on particles, as in [32]. The right boundary is a conductor that collects charged particles. When particles hit the right boundary, they are removed from the simulation. Since electrons have a higher average velocity than ions, they have a greater flux on the collector and become depleted near the right boundary, where the difference between ion and electron densities leads to a collector sheath region, where the potential changes from the interior value to the wall value, which has the effect of repelling electrons away from the right wall. Electrons and ions are replenished by a particle source region near the left boundary, where electrons and ions are

injected uniformly in the region from a Maxwellian distribution at a fixed rate per time step. We take $m_i/m_e = 100$, $T_{src,i}/T_{src,e} = 1$, and we set $v_{th,e} = 1$, and set $L_x = 20$ (in Debye lengths). We use a 100 cell grid and take $\Delta t = 0.1$, which gives a CFL number of 50. We run our simulation for 8000 time steps, up to 3.6 thermal-ion transit times. In Figure 7 we see the result of the simulation. In Figure 7a, we see the profile of the potential, which has the right qualitative features, including a collector sheath region that is several Debye lengths wide. In Figure 7b, we see the net electron and ion counts, along with the injection rate. The difference between the electron and ion counts reflects the difference between electron and ion densities in the collector sheath region.

5.2. **Electromagnetic Test Problems.**

5.2.1. *Bennett Pinch Problem.* We present the application of our PIC method to the Bennett pinch [3], an effect related to the magnetic confinement of a beam of charged particles. A beam of charged particles induces a solenoidal magnetic field around the beam. Particles near the edge of the beam move orthogonally to these field lines at the beam drift velocity, causing the particles to be accelerated towards the center of the beam, in effect confining particles in the beam. An appropriate choice of parameters leads to a stationary steady state, uniform along the axis of the beam. A well-known magnetohydrodynamic (MHD) model of a stationary steady state gives explicit formulas for the beam density and the magnetic field [5], and provides a basis for the validation of our numerical method. Moreover, it is a first step toward applying our method to more physically interesting beam instability problems in three dimensions.

Our PIC simulation of the Bennett pinch is two-dimensional in physical space, and three-dimensional in velocity space. The particle beam is considered uniform along the axis of the beam, which we take to be the z-direction, which reduces the physical dimensions to two. Electrons drift in the z-direction with a uniform average beam drift velocity v_b, and this motion induces a confining magnetic field with only x- and y-components. A stationary ion background distribution enforces quasineutrality in the beam, with any separation of charge producing an electric field with only x- and y-components acting as a restoring force. The electrons are assumed to follow a Maxwellian distribution with thermal velocity v_{th}. We take $v_b/v_{th} = 100$ and $c/v_{th} = 1000$, where c is the speed of light. The ions are considered cold ($T_i = 0$).

Since the beam drift velocity is taken to be much larger than the (transverse) thermal velocity, and further, the transverse velocities follow a Maxwellian distribution and so should not generate any net currents, we neglect the x- and y-components of the current density (and so also of $\mathbf{A}$). In the true solution, $\frac{\partial \Phi}{\partial z} = 0$ and $\frac{\partial A_z}{\partial t} = 0$, so we neglect $E_z = -\frac{\partial \Phi}{\partial z} - \frac{\partial A_z}{\partial t}$. Hence, we actually only solve two wave equation, one for A_z, obtaining only transverse magnetic field components, $B_x = \frac{\partial A_z}{\partial y}$ and $B_y = -\frac{\partial A_z}{\partial x}$, and one for Φ, obtaining only transverse electric field components $E_x = -\frac{\partial \Phi}{\partial x}$ and $E_y = -\frac{\partial \Phi}{\partial y}$. Thus, the Poisson equation satisfied by the scalar potential is $-\Delta\Phi = \rho/\epsilon_0$. We discretize our domain with a staggered grid, one cell of which is shown in Figure 8.

The scalar potential is calculated from the standard 5-point finite difference Laplacian, and satisfies the equation

$$-\frac{\Phi^{i+1,j}+\Phi^{i,j+1}+\Phi^{i-1,j}+\Phi^{i,j-1}-4\Phi^{i,j}}{\Delta x^2}=\rho^{i,j}/\epsilon_0.$$

The electric and magnetic fields are calculated on the staggered grid by finite differences as

$$\begin{aligned}
E_x^{i+1/2,j} &= -\frac{\Phi^{i+1,j}-\Phi^{i,j}}{\Delta x}\\
E_y^{i,j+1/2} &= -\frac{\Phi^{i,j+1}-\Phi^{i,j}}{\Delta x}\\
B_x^{i,j+1/2} &= \frac{A_z^{i,j+1}-A_z^{i,j}}{\Delta x}\\
B_y^{i+1/2,j} &= -\frac{A_z^{i+1,j}-A_z^{i,j}}{\Delta x}.
\end{aligned}$$

The electric field then satisifies the following discrete analogue of Gauss' law:

$$\begin{aligned}
[\nabla\cdot\mathbf{E}]^{i,j} &= \frac{E_x^{i+1/2,j}-E_x^{i-1/2,j}}{\Delta x}+\frac{E_y^{i,j+1/2}-E_y^{i,j-1/2}}{\Delta x}\\
&= \frac{1}{\Delta x}\left(\left(-\frac{\Phi^{i+1,j}-\Phi^{i,j}}{\Delta x}\right)-\left(-\frac{\Phi^{i,j}-\Phi^{i-1,j}}{\Delta x}\right)+\right.\\
&\left.+\left(-\frac{\Phi^{i,j+1}-\Phi^{i,j}}{\Delta x}\right)-\left(-\frac{\Phi^{i,j}-\Phi^{i,j-1}}{\Delta x}\right)\right)\\
&= -\frac{\Phi^{i+1,j}+\Phi^{i,j+1}+\Phi^{i-1,j}+\Phi^{i,j-1}-4\Phi^{i,j}}{\Delta x^2}\\
&= \rho^{i,j}/\epsilon_0.
\end{aligned}$$

The magnetic field satisfies the following discrete analogue of the divergence free condition:

$$\begin{aligned}
[\nabla\cdot\mathbf{B}]^{i+1/2,j+1/2} &= \frac{B_x^{i+1,j+1/2}-B_x^{i,j+1/2}}{\Delta x}+\frac{B_y^{i+1/2,j+1}-B_y^{i+1/2,j}}{\Delta x}\\
&= \frac{1}{\Delta x}\left(\left(\frac{A_z^{i+1,j+1}-A_z^{i+1,j}}{\Delta x}\right)-\left(\frac{A_z^{i,j+1}-A_z^{i,j}}{\Delta x}\right)+\right.\\
&\left.+\left(-\frac{A_z^{i+1,j+1}-A_z^{i,j+1}}{\Delta x}\right)-\left(-\frac{A_z^{i+1,j}-A_z^{i,j}}{\Delta x}\right)\right)\\
&= 0.
\end{aligned}$$

All computational boundaries in this problem are outflow boundaries. In order to supply the finite difference Poisson solver with suitable boundary values, the wave solver is applied with outflow boundaries conditions to evolve the wave potential Φ_W alongside the Poisson potential Φ. The boundary values from Φ_W are then supplied to the Poisson solver to use in calculating Φ. Once the wave solver reaches steady state, Φ_W and Φ differ only by 0.1% relative error, however, the wave potential gives a discrete electric field with divergence error on the order of 10^{-3}, while the Poisson potential gives a discrete electric field with divergence error on the order of machine epsilon 10^{-16}.

Like in the other test problems, we use the diffusive version of wave solver. Particle velocities in all three directions are updated with the nonrelativistic Boris push [4]. Particles are initialized according to the MHD steady state (according to the theoretical spatial density profile and the corresponding Maxwellian distribution in velocity space) and held fixed while the field solver is stepped to an approximate steady state, after which the particle push is turned on. The simulation is run to a final time of $R_b/(2v_{th})$ (plus startup time), where R_b is an effective beam radius and v_{th} is the thermal velocity, at which time there would be substantial spreading of the beam in absence of the confinement effect. We choose R_b such that 99% of the particles in the theoretical beam are within this radius. In loading particles, the beam is cut off at radius R_b (no particles are loaded outside of this radius). The computational domain is taken to be a $4R_b \times 4R_b$ square centered on the beam axis. The computational domain is truncated with outflow boundary conditions. Particles exiting the boundary of the computational domain are reinjected into the beam to maintain constant total current. However, since most particles should be confined within the beam, such boundary crossings should be rare.

Numerical results for the Bennett pinch are given in Figure 9. In order to resolve large gradients near the center of the beam, we use a 500-cell by 500-cell grid and a CFL number of $c\Delta t/\Delta x = 3$ (except in Figure 9c as noted) and 500,000 electron particles. Final numerical solutions are shown at the final time, after 334 start up time steps and 20,834 PIC time steps. (The final time is approx. 22 plasma periods, and the diameter of the beam is approx. 280 Debye lengths.) In Figure 9a, we see good agreement between the numerical electron density and MHD theory. The inset zoomed portion shows a slight discrepency at the peak of the beam, due to statistical fluctuation caused by the finite number of particles. In Figure 9b, we see the time histories of the potential energy, calculated as $\sum_j \frac{\Delta x \Delta y}{2}\left[\frac{1}{\mu_R}(B_{x,j}^2 + B_{y,j}^2) + \varepsilon_R(E_{x,j}^2 + E_{y,j}^2)\right]$ where the sum is over grid points j (with ε_R and μ_R defined as in Section 7.1.2), and the kinetic energy, calculated as $\sum_i \frac{1}{2}m_i(v_{x,i}^2 + v_{y,i}^2 + (v_{x,i} - v_b)^2)$ where the sum is over electron particles i. We see good energy conservation, despite the slight dissipation of the diffusive scheme. The initial spike in the potential energy is the result of transient waves, arising due to the beam turning on, and flowing out of the domain as the solution is stepped to a steady state. In Figure 9c, we see the result of refinement in Δt, keeping Δx fixed, showing a profile of the azimuthal magnetic field B_θ along the central $y = 0$ slice for CFL numbers of 3, 10 and 20, along with MHD theory. We observe approximate second-order convergence in Δt, as expected (a more robust convergence study is confounded by the slow convergence in particle number in PIC methods). Outside of the beam radius $R_b = 1$, there is error associated with the finite cut-off radius of the beam (the theoretical beam density decays only algebraically). In Figure 9d, we see the numerical error of the azimuthal magnetic field B_θ (with a CFL number of of 3) normalized by the peak value of the magnetic field, and we see that there is a geometric pattern to the numerical error, characteristic of the dimensionally-split method. In addition to this splitting error, the total error is contributed to by errors associated with the spatial quadrature and the finite differences used to calculate the magnetic field (likely contributing to the large error at the center of the beam due to large gradients there) and with the finite beam cut-off radius and the outflow boundary condition (contributing most strongly near the boundary of the computational domain). These results show that our method can indeed simulate a basic electromagnetic plasma phenomenon with a CFL number larger than what

is allowed by typical explicit schemes. The CFL number used in this problem is limited by the accuracy of the second-order wave solver. A higher-order wave solver, such as those in [9], would allow for a larger usable time step size, and will be the subject of further investigation.

5.2.2. *Mardahl Beam Problem.* We apply our method to the beam problem proposed in [26] as a diagnostic for the effects of divergence error.

In the Mardahl beam problem, we have currents in the plane of simulation only, and so we retain the x- and y-components of the vector potential, A_x and A_y, along with the scalar potential Φ in the model. We retain the electric field components $E_x = -\frac{\partial \Phi}{\partial x} - \frac{\partial A_x}{\partial t}$ and $E_y = -\frac{\partial \Phi}{\partial y} - \frac{\partial A_y}{\partial t}$ and the magnetic field component $B_z = \frac{\partial A_y}{\partial x} - \frac{\partial A_x}{\partial y}$. The Poisson equation satisfied by the scalar potential is

$$-\Delta \Phi = \rho/\epsilon_0 + \frac{\partial}{\partial t}\left(\frac{\partial A_x}{\partial x} + \frac{\partial A_y}{\partial y}\right)$$

We discretize our domain with a staggered grid, one cell of which is shown in Figure 10.

Denoting by $D_{\Delta t}$ a (linear) finite difference discretization of the time derivative operator $\partial/\partial t$, the scalar potential satisfies the equation

$$-\frac{\Phi^{i+1,j} + \Phi^{i,j+1} + \Phi^{i-1,j} + \Phi^{i,j-1} - 4\Phi^{i,j}}{\Delta x^2} = \rho^{i,j}/\epsilon_0 + D_{\Delta t}\left(\frac{A_x^{i+1/2,j} - A_x^{i-1/2,j}}{\Delta x} + \frac{A_y^{i,j+1/2} - A_y^{i,j-1/2}}{\Delta x}\right).$$

The electric and magnetic fields are calculated on the staggered grid by finite differences as

$$\begin{aligned} E_x^{i+1/2,j} &= -\frac{\Phi^{i+1,j} - \Phi^{i,j}}{\Delta x} - D_{\Delta t}(A_x^{i+1/2,j}) \\ E_y^{i,j+1/2} &= -\frac{\Phi^{i,j+1} - \Phi^{i,j}}{\Delta y} - D_{\Delta t}(A_y^{i,j+1/2}) \\ B_z^{i+1/2,j+1/2} &= \frac{A_y^{i+1,j} - A_y^{i,j}}{\Delta x} - \frac{A_x^{i,j+1} - A_x^{i,j}}{\Delta y} \end{aligned}$$

The electric field then satisifies the following discrete analogue of Gauss' law:

$$
\begin{aligned}
[\nabla \cdot \mathbf{E}]^{i,j} &= \frac{E_x^{i+1/2,j} - E_x^{i-1/2,j}}{\Delta x} + \frac{E_y^{i,j+1/2} - E_y^{i,j-1/2}}{\Delta y} \\
&= \frac{1}{\Delta x}\left(\left(-\frac{\Phi^{i+1,j} - \Phi^{i,j}}{\Delta x} - D_{\Delta t}(A_x^{i+1/2,j})\right) - \left(-\frac{\Phi^{i,j} - \Phi^{i-1,j}}{\Delta x} - D_{\Delta t}(A_x^{i-1/2,j})\right) + \right. \\
&\left. + \left(-\frac{\Phi^{i,j+1} - \Phi^{i,j}}{\Delta x} - D_{\Delta t}(A_y^{i,j+1/2})\right) - \left(-\frac{\Phi^{i,j} - \Phi^{i,j-1}}{\Delta x} - D_{\Delta t}(A_y^{i,j-1/2})\right)\right) \\
&= -\frac{\Phi^{i+1,j} + \Phi^{i,j+1} + \Phi^{i-1,j} + \Phi^{i,j-1} - 4\Phi^{i,j}}{\Delta x^2} - \\
&D_{\Delta t}\left(\frac{A_x^{i+1/2,j} - A_x^{i-1/2,j}}{\Delta x} + \frac{A_y^{i,j+1/2} - A_x^{i,j-1/2}}{\Delta x}\right) \\
&= \rho^{i,j}/\epsilon_0.
\end{aligned}
$$

where we have used the linearity of $D_{\Delta t}$.

6. Conclusions and Future Work

In this work, we have described a PIC method that uses an unconditionally stable wave equation solver to eliminate the CFL restriction on the ratio of the time step size to the spatial step size, typical of explicit methods, while retaining computational cost and code complexity comparable to such explicit methods. Our numerical results show that we can apply our method to problems of plasma physics using a time step size larger than what would be allowed by a typical explicit field solver. We have seen that the usable time step size can be limited by the numerical accuracy of the method when there are large gradients (high-frequency content) in the solution. We implement a staggered grid approach to give an electromagnetic PIC method that satisfies exactly a discrete form of Gauss' law. Future work will center on making use of the implicit wave solvers ability to handle complex boundary geometries without the use of a staircasing approximation. We will investigate the use of higher-order methods, such as given in [9], in our PIC method in order to increase the maximum usable time step size (we have already found a 4th order Newmark scheme with slight dissipation that may prove useful). A further course of action will be to implement a boundary integral treecode (BIT) solution to solve the modified Helmholtz equations in the semi-discrete schemes, such as in [24], rather than use dimensional splitting.

7. Appendix

7.1. **Nondimensionalization and Asymptotic Analysis.** We provide the normalizations used in the test problems presented in this work in both electrostatic and electromagnetic cases. In the electrostatic case, we argue by formal asymptotic analysis and classical solution formulas that the Vlasov-Wave system agrees with the Vlasov-Poisson system in the relevant scaling limit.

7.1.1. *Electrostatic Case.* Here we give the normalization used for the electrostatic test problems in Section 5.1. Consider the following change of variables:

$$
\tilde{f} = Ff, \quad \tilde{t} = Tt, \quad \tilde{\mathbf{x}} = L\mathbf{x}, \quad \tilde{\mathbf{v}} = V\mathbf{v}, \quad \tilde{\rho} = qN\rho, \quad \tilde{\Phi} = \Phi_0\Phi
$$

applied to the system

$$\frac{\partial \tilde{f}}{\partial \tilde{t}} + \tilde{\mathbf{v}} \cdot \nabla_{\tilde{\mathbf{x}}} \tilde{f} - \frac{q}{m} \nabla \tilde{\Phi} \cdot \nabla_{\tilde{\mathbf{v}}} \tilde{f} = 0$$

$$\frac{1}{c^2} \frac{\partial^2 \tilde{\Phi}}{\partial \tilde{t}^2} - \Delta \tilde{\Phi} = \tilde{\rho}/\varepsilon_0, \quad \tilde{\rho}(\tilde{\mathbf{x}}, \tilde{t}) = q \int_{\tilde{\mathbf{v}}} \tilde{f}(\tilde{\mathbf{x}}, \tilde{\mathbf{v}}, \tilde{t}) d\tilde{\mathbf{v}}$$

Assuming the scalings,

$$V = \frac{L}{T}, \quad T = \sqrt{\frac{m\varepsilon_0}{Nq^2}} = \omega_p^{-1}, \quad \Phi_0 = \frac{qNL^2}{\varepsilon_0}, \quad F = \frac{N^{\frac{2-d}{d}} (\varepsilon_0 m)^{d/2}}{q^d L^d},$$

which are the natural scalings in the electrostatic limit, we obtain:

$$\frac{\partial f}{\partial t} + \mathbf{v} \cdot \nabla_{\mathbf{x}} f - \nabla \Phi \cdot \nabla_{\mathbf{v}} f = 0$$

$$\epsilon^2 \frac{\partial^2 \Phi}{\partial t^2} - \Delta \Phi = \rho, \quad \rho(\mathbf{x}, t) = \int_{\mathbf{v}} f(\mathbf{x}, \mathbf{v}, t)\, d\mathbf{v}$$

where $\epsilon = \frac{L}{cT} = \frac{V}{c}$ (not to be confused with the electric permittivity ε_0). Note that $1/\epsilon$ is the speed of propagation of waves in the potential in this normalization, and becomes large when ϵ is small, that is, when the characteristic particle velocities are small compared to the speed of light.

Assume the following formal asymptotic expansions:

$$\begin{aligned}
f &= f_0 + \epsilon f_1 + \epsilon^2 f_2 + \cdots \\
\rho &= \int_{\mathbf{v}} f d\mathbf{v} \\
&= \int_{\mathbf{v}} f_0 d\mathbf{v} + \epsilon \int_{\mathbf{v}} f_1 d\mathbf{v} + \epsilon^2 \int_{\mathbf{v}} f_2 d\mathbf{v} + \cdots \\
&= \rho_0 + \epsilon \rho_1 + \epsilon^2 \rho_2 + \cdots \\
\Phi &= \Phi_0 + \epsilon \Phi_1 + \epsilon^2 \Phi_2 + \cdots
\end{aligned}$$

Collecting in orders of ϵ:

$$
\begin{aligned}
O(1): \quad & \frac{\partial f_0}{\partial t} + \mathbf{v}\cdot\nabla_{\mathbf{x}} f_0 - \nabla\Phi_0\cdot\nabla_{\mathbf{v}} f_0 = 0 \\
& -\Delta\Phi_0 = \rho_0, \quad \rho_0 = \int_{\mathbf{v}} f_0\, d\mathbf{v} \\
O(\epsilon): \quad & \frac{\partial f_1}{\partial t} + \mathbf{v}\cdot\nabla_{\mathbf{x}} f_1 - \nabla\Phi_0\cdot\nabla_{\mathbf{v}} f_1 - \nabla\Phi_1\cdot\nabla_{\mathbf{v}} f_0 = 0 \\
& -\Delta\Phi_1 = \rho_1, \quad \rho_1 = \int_{\mathbf{v}} f_1\, d\mathbf{v} \\
O(\epsilon^k), \quad k\geq 2: \quad & \frac{\partial f_k}{\partial t} + \mathbf{v}\cdot\nabla_{\mathbf{x}} f_k - \sum_{j=0}^{k} \nabla\Phi_j\cdot\nabla_{\mathbf{v}} f_{k-j} = 0 \\
& -\Delta\Phi_k = \rho_k - \frac{\partial^2\Phi_{k-2}}{\partial t^2}, \quad \rho_k = \int_{\mathbf{v}} f_k\, d\mathbf{v}
\end{aligned}
$$

We note that the leading order is precisely the Vlasov-Poisson system (nondimensionalized under the same scalings). This formal computation suggests that our model will agree with the electrostatic model to $O(\epsilon = V/c)$ when particle velocities are small compared to the speed of light. This can be considered as a consequence of the strong Huygens' principle in odd spatial dimensions, and of a weaker decay property that holds in even spatial dimensions, which can be deduced from classical solution formulas [15, 30]. Consider the Cauchy problem,

$$
\begin{aligned}
\frac{1}{c^2}\frac{\partial^2 u}{\partial t^2} - \Delta u = f(x,t) \qquad & (x,t)\in\mathbb{R}^d\times(0,\infty) \\
u(x,0) = 0 \qquad & x\in\mathbb{R}^d \\
u_t(x,0) = 0 \qquad & x\in\mathbb{R}^d
\end{aligned}
$$

for $d = 2, 3$ and f sufficiently smooth with compact support, for which classical explicit solution formulas exist. We consider the case of f having compact support in $B(0,R)\times(0,T)\subset\mathbb{R}^d\times(0,\infty)$, where $B(0,R) = \{x\in\mathbb{R}^d | \sum_{j=1}^{d} x_j^2 < R^2\}$. Classical solution formulas imply that for $x\in B(0,R)$ and $t > T + 2R/cT$, we have

$$
\begin{aligned}
u(x,t) = O((ct)^{-1}) \qquad & d = 2 \\
u(x,t) = 0 \qquad & d = 3
\end{aligned}
$$

As a generalization of this, for any sufficiently smooth $f(\cdot,t)$ supported in $B(0,R)$ for all $t > 0$ with $f(\cdot,t) = f_T(\cdot)$ for all $t > T$, it is again easily argued that for $x\in B(0,R)$ and $t > T + 2R/cT$, we have

$$
\begin{aligned}
u(x,t) = u_P^2(x) + O((ct)^{-1}) \qquad & d = 2 \\
u(x,t) = u_P^3(x) \qquad & d = 3
\end{aligned}
$$

where $u_P^d(x)$ is the classical integral solution of the Poisson equation $-\Delta u_P^d = f_T$ in dimension d.

The convergence of solutions to the Vlasov-Maxwell system to those of the Vlasov-Poisson system has been rigorously considered in works such as [2, 34]. It may be possible to apply similar techniques to rigorously study the convergence of solutions of our Vlasov-Wave model to those of the Vlasov-Poisson system, but this is outside of the scope of the present work.

7.1.2. *Electromagnetic Case.* Here we give the normalization used for the electromagnetic test problem in Section 5.2.1. Consider the following change of variables:

$$\begin{aligned}
&\tilde{f} = Ff, \quad \tilde{t} = Tt, \quad \tilde{\mathbf{x}} = L\mathbf{x}, \quad \tilde{\mathbf{v}} = V\mathbf{v}, \\
&\tilde{\rho} = qN\rho, \quad \tilde{J}_z = qVNJ_z, \\
&\tilde{\Phi} = \Phi_0\Phi, \quad \tilde{\mathbf{A}} = A_0 A_z
\end{aligned}$$

applied to the system

$$\frac{\partial \tilde{f}}{\partial \tilde{t}} + \tilde{\mathbf{v}} \cdot \nabla_{\tilde{\mathbf{x}}} \tilde{f} + \frac{q}{m}\left(-\nabla_{\tilde{\mathbf{x}}}\tilde{\Phi} - \tilde{\mathbf{v}} \times (\nabla_{\tilde{\mathbf{x}}} \times (0,0,\tilde{A}_z))\right) \cdot \nabla_{\tilde{\mathbf{v}}} \tilde{f} = 0$$

$$\frac{1}{c^2}\frac{\partial^2 \tilde{\Phi}}{\partial \tilde{t}^2} - \Delta \tilde{\Phi} = \tilde{\rho}/\varepsilon_0, \qquad \tilde{\rho}(\tilde{\mathbf{x}}, \tilde{t}) = q\int_{\tilde{\mathbf{v}}} \tilde{f}(\tilde{\mathbf{x}}, \tilde{\mathbf{v}}, \tilde{t}) d\tilde{\mathbf{v}}$$

$$\frac{1}{c^2}\frac{\partial^2 \tilde{A}_z}{\partial \tilde{t}^2} - \Delta \tilde{A}_z = \mu_0 \tilde{J}_z, \qquad \tilde{J}_z(\tilde{\mathbf{x}}, \tilde{t}) = q\int_{\tilde{\mathbf{v}}} \tilde{v}_z \tilde{f}(\tilde{\mathbf{x}}, \tilde{\mathbf{v}}, \tilde{t}) d\tilde{\mathbf{v}}$$

Assuming the scalings,

$$\begin{aligned}
&V = \frac{L}{T}, \quad T = \sqrt{\frac{m\varepsilon_0}{Nq^2}} = \omega_p^{-1}, \\
&\Phi_0 = \frac{qNL^2\varepsilon_R}{\varepsilon_0}, \quad A_0 = \frac{\mu_0 V q N L^2}{\mu_R}, \quad \varepsilon_R\mu_R = V^2/c^2, \\
&F = \frac{N^{\frac{2-d}{d}}(\varepsilon_0 m)^{d/2}}{q^d L^d}
\end{aligned}$$

where ε_R and μ_R are dimensionless parameters introduced to enforce the Lorenz gauge condition, we obtain:

$$\frac{\partial f}{\partial t} + \mathbf{v} \cdot \nabla_{\mathbf{x}} f + \varepsilon_R(-\nabla\Phi + \mathbf{v} \times (\nabla \times (0,0,A_z)) \cdot \nabla_{\mathbf{v}} f = 0$$

$$\epsilon^2 \frac{\partial^2 \Phi}{\partial t^2} - \Delta\Phi = \rho/\varepsilon_R, \quad \rho(\mathbf{x}, t) = \int_{\mathbf{v}} f(\mathbf{x}, \mathbf{v}, t)\, d\mathbf{v}$$

$$\epsilon^2 \frac{\partial^2 A_z}{\partial t^2} - \Delta A_z = \mu_R J_z, \quad J_z(\mathbf{x}, t) = \int_{\mathbf{v}} v_z f(\mathbf{x}, \mathbf{v}, t)\, d\mathbf{v}$$

where $\epsilon = \frac{L}{cT} = \frac{V}{c}$, as in the electrostatic case. For the Bennett pinch problem in Section 5.2.1, we choose $\varepsilon_R = 1$.

7.2. **Semi-Discrete Von Neumann Analysis.** In this section, we provide semi-discrete Von Neumann stability analyses and dispersion relations for the semi-discrete schemes derived in 3. These build on similar analyses for related, but different, schemes given in [8].

7.2.1. *Diffusive Scheme.* Substituting the ansatz $u^n = e^{i(k\cdot x - \tilde{\omega} n\Delta t)}$ into

$$\left(-\frac{1}{\alpha^2}\Delta + 1\right) u^{n+1} = \frac{1}{2}\left(5u^n - 4u^{n-1} + u^{n-2}\right),$$

we obtain a polynomial

$$\lambda^3 - 4\lambda^2 + 5\lambda - 2(1+z^2) = 0$$

where $\lambda = e^{i\tilde{\omega}\Delta t}$, $z = |k|/\alpha$. The three roots tell us about possible modes $u^n = e^{ik\cdot x}\lambda^{-n}$.

A necessary condition for stability is $\lambda \geq 1$ for all roots.

The first root,

$$\lambda_1 = \frac{4}{3} + \frac{1}{3}\left(27z^2 + 3\sqrt{3}\sqrt{27z^4 + 2z^2} + 1\right)^{1/3} + \frac{1}{3\left(27z^2 + 3\sqrt{3}\sqrt{27z^4 + 2z^2} + 1\right)^{1/3}},$$

corresponds to a spurious nonpropagating mode of the form $u^n = e^{ik\cdot x}\lambda_1^{-n}$. Since $\lambda_1 \geq 2$ for all $z = |k|c\Delta t/\sqrt{2} \geq 0$, the mode rapidly decays and poses no threat to stability.

The other two roots are a pair of complex conjugates:

$$\begin{aligned}\lambda_{2/3} &= -\frac{1}{6}(1 \mp i\sqrt{3})\left(27z^2 + 3\sqrt{3}\sqrt{27z^4 + 2z^2} + 1\right)^{1/3} - \\ &\quad - \frac{1 \pm i\sqrt{3}}{6(27z^2 + 3\sqrt{3}\sqrt{27z^4 + 2z^2} + 1)^{1/3}} + 4/3 \\ &\approx 1 \pm i\sqrt{2}z - z^2 \mp i\frac{5\sqrt{2}}{4}z^3 + 4z^4 \pm i\frac{231\sqrt{2}}{32}z^5 + O(z^6) \text{ as } z \to 0.\end{aligned}$$

We can show that

$$|\lambda_{2/3}|^2 = \frac{16}{9} + \frac{4W^4 - 16W^3 - 4W^2 - 16W + 4}{36W^2} \geq 1 \quad \text{for all } W \geq 1$$

where $W = \left(27z^2 + 3\sqrt{3}\sqrt{27z^4 + 2z^2} + 1\right)^{1/3} \geq 1$ for all $z \geq 0$.

Since $\lambda = e^{i\tilde{\omega}\Delta t}$, we have

$$\begin{aligned}\tilde{\omega} &= \frac{1}{i\Delta t}\log(\lambda) \\ &\approx \frac{1}{i\Delta t}\log(1 + i\sqrt{2}z - z^2 - i\frac{5\sqrt{2}}{4}z^3 + 4z^4 + i\frac{231\sqrt{2}}{32}z^5 + O(z^6)) \\ &\approx |k|c\left(1 - \frac{11(|k|c\Delta t)^2}{24} - i\frac{(|k|c\Delta t)^3}{2} - \frac{15(|k|c\Delta t)^4}{16} + O((|k|c\Delta t)^5)\right)\end{aligned}$$

So the phase error is $|\frac{\tilde{\omega}}{|k|c} - 1| = O((|k|c\Delta t)^2)$.

The presence of the imaginary third term in the expansion shows that $u^n \sim e^{-in(-i(|k|c\Delta t)^3)\Delta t)} = e^{-n(|k|c)^3\Delta t^4/2}$, causing the mode to decay. This is why we term this scheme diffusive (or dissipative).

7.2.2. *Dispersive Scheme.* Substitute ansatz $u^n = e^{i(k\cdot x - \tilde{\omega} n\Delta t)}$ into

$$\left(-\frac{1}{\alpha^2}\Delta + 1\right)\left(u^{n+1} + 2u^n + u^{n-1}\right) = 4u^n$$

Obtain a polynomial

$$\lambda^2 + 2\left(\frac{|k|^2 - \alpha^2}{|k|^2 + \alpha^2}\right)\lambda + 1 = 0$$

where $\lambda = e^{i\tilde{\omega}\Delta t}$.

We can solve to obtain $\lambda_{1/2} = \frac{\alpha \pm i|k|}{\alpha \mp i|k|}$, which gives $|\lambda_{1/2}| = 1$, meaning this scheme is non-dissipative.

Noting that $\cos(\tilde{\omega}\Delta t) = \frac{1}{2}(\lambda_1 + \lambda_2)$, and defining $z = |k|/\alpha = |k|c\Delta t/2$, we obtain

$$\begin{aligned}
\tilde{\omega} &= \frac{2}{\Delta t}\arccos\left(\sqrt{\frac{\alpha^2}{|k|^2 + \alpha^2}}\right) = \frac{2}{\Delta t}\arccos\left(\sqrt{\frac{1}{1+z^2}}\right) \\
&\approx \frac{2}{\Delta t}\left(z - z^3/3 + O(z^5)\right) \\
&\approx |k|c\left(1 - \frac{1}{12}\left(|k|c\Delta t\right)^2 + O((|k|c\Delta t)^4)\right)
\end{aligned}$$

So the phase error is $|\frac{\tilde{\omega}}{|k|c} - 1| = O((|k|c\Delta t)^2)$. Moreover, $\tilde{\omega}$ is real, owing to the non-dissipative nature of the scheme.

7.3. **Fully Discrete Von Neumann Analysis.** In this section, we provide fully discrete Von Neuman analyses for the two fully discrete schemes derived in 3, and show that they are unconditionally stable, in the sense of Von Neumann analysis. Combining the quadrature rules and exponential recursion, and ignoring boundaries, we can write

$$\begin{aligned}
I[f](x_j) = \frac{\alpha}{2}\int_{-\infty}^{\infty} f(x')e^{-\alpha|x_j - x'|}\,dx' \approx \\
\approx I_h[f_j] = Pf_j + \frac{1}{2}Q\left(f_{j+1} + f_{j-1}\right) + R\left(f_{j+1} - 2f_j + f_{j-1}\right) + \\
+ \frac{1}{2}\sum_{k=1}^{\infty} e^{-\nu k}\left[P\left(f_{j+k} + f_{j-k}\right) + Q\left(f_{j+k+1} + f_{j-k-1}\right) + \right. \\
\left. + R\left(f_{j+k+1} - 2f_{j+k} + f_{j+k-1} + f_{j-k+1} - 2f_{j-k} + f_{j-k-1}\right)\right]
\end{aligned}$$

with $\nu = \alpha h = \alpha\Delta x$ and P, Q, and R defined as in Section 3.

Using the discrete convolution operator I_h, and ignoring sources and boundaries, we can write the diffusive version of the fully discrete scheme as

$$u_j^{n+1} = \frac{1}{2}I_h[5u_j^n - 4u_j^{n-1} + u_j^{n-2}]$$

and the dispersive scheme as

$$u_j^{n+1} + 2u_j^n + u_j^{n-1} = 4I_h[u_j^n]$$

Defining $I_{h,x}$ and $I_{h,y}$ as the discrete convolution operators acting in the x- and y-directions, and again ignoring sources and boundaries, we can write the diffusive version of the 2D fully discrete scheme as

$$u_{jk}^{n+1} = \frac{1}{2} I_{h,x}[I_{h,y}[5u_{jk}^{n} - 4u_{jk}^{n-1} + u_{jk}^{n-2}]]$$

and the 2D fully dispersive scheme as

$$u_{jk}^{n+1} + 2u_{jk}^{n} + u_{jk}^{n-1} = 4I_{h,x}[I_{h,y}[u_{jk}^{n}]]$$

We will refer to these as free-space schemes. We now state a stability theorem based on the Von Neumann analysis of the schemes.

Theorem. *The fully discrete dispersive and diffusive free-space schemes in one dimension are unconditionally stable. In higher dimensions, the corresponding dimensionally-split schemes are also unconditionally stable.*

To prove the stability theorem, we consider some properties of the discrete covolution operator.

Lemma. *Define the amplification factor* $A(\tilde{k}, \nu) = e^{-i\tilde{k}j\Delta x} I_h[e^{i\tilde{k}j\Delta x}]$. *Then* $A(\tilde{k}, \nu)$ *is well-defined (independent of* j*), and the following hold.*

- *If* $\nu > 0$ *and* $0 < |\tilde{k}\Delta x| \leq \pi$, *then* $0 < A(\tilde{k}, \nu) < 1$.
- *If* $\nu > 0$, *then* $A(0, \nu) = 1$.
- *For any* $0 < |\tilde{k}\Delta x| \leq \pi$, $\lim_{\nu \to 0^+} A(\tilde{k}, \nu) = 0$.
- *For any* $0 < |\tilde{k}\Delta x| \leq \pi$, $\lim_{\nu \to \infty} A(\tilde{k}, \nu) = 1$.

Proof of the Lemma. We calculate:

$$\begin{aligned} A(\tilde{k}, \nu) =& e^{-i\tilde{k}j\Delta x} I_h[e^{i\tilde{k}j\Delta x}] \\ =& P\left(1 + \sum_{k=1}^{\infty} e^{-k\nu} \cos(k\tilde{k}\Delta x)\right) + \\ &+ Q\left(e^{\nu} \sum_{k=1}^{\infty} e^{-k\nu} \cos(k\tilde{k}\Delta x)\right) + \\ &+ 2R(\cos(\tilde{k}\Delta x) - 1)\left(1 + \sum_{k=1}^{\infty} e^{-k\nu} \cos(k\tilde{k}\Delta x)\right) \\ =& 1 + T, \end{aligned}$$

$$T = \frac{\frac{d^2+d}{\nu}(\cos(\tilde{k}\Delta x) - 1)^2 - 2\frac{1-d}{\nu^2}(d\cos(\tilde{k}\Delta x) - 1)(\cos(\tilde{k}\Delta x) - 1)}{d^2 - 2\cos(\tilde{k}\Delta x)d + 1}$$

with $d = e^{-\nu}$.

If $\tilde{k}\Delta x = 0$ and $\nu > 0$, then $T = 0$. If $0 < |\tilde{k}\Delta x| \leq \pi$, some calculus shows $-1 < T < 0$ for any $\nu > 0$, and $\lim_{\nu \to 0^+} T = -1$, and $\lim_{\nu \to \infty} T = 0$. □

Proof of the Theorem. We first prove that each one-dimensional free-space fully discrete scheme is unconditionally stable, then describe the extension of the result to multiple dimensions for the dimensionally-split schemes.

Diffusive Scheme

Consider applying the fully discrete diffusive scheme to $u_j^n = e^{i(\tilde{k}j\Delta x - \tilde{\omega}n\Delta t)}$. We obtain a polynomial

$$\lambda^3 - 4\lambda^2 + 5\lambda - z = 0$$

where $\lambda = e^{i\tilde{\omega}\Delta t}$ and $z = 2/A(\tilde{k}, \nu)$. Note that the lemma implies $z \geq 2$ for all $\tilde{k}$ and $\Delta x, \Delta t > 0$. The condition for stability is $|\lambda| \geq 1$ for all roots of the polynomial, which we verify below.

The first root corresponds to a spurious mode:

$$\lambda_1 = \frac{4}{3} + \frac{\sqrt[3]{3\sqrt{3}\sqrt{27z^2 - 104z + 100} + 27z - 52}}{3\sqrt[3]{2}} + \\ + \frac{\sqrt[3]{2}}{3\sqrt[3]{3\sqrt{3}\sqrt{27z^2 - 104z + 100} + 27z - 52}}$$

We can show that

$$\lambda_1 = \frac{W^2 + 4W + 1}{3W} \geq 2 \quad \text{for all } W \geq 1$$

where $W = \frac{\sqrt[3]{3\sqrt{3}\sqrt{27z^2 - 104z + 100} + 27z - 52}}{\sqrt[3]{2}} \geq 1$ for $z \geq 2$.

The other roots are pair of complex conjugates:

$$\lambda_{2/3} = \frac{4}{3} - (1 \mp i\sqrt{3})\frac{\sqrt[3]{3\sqrt{3}\sqrt{27z^2 - 104z + 100} + 27z - 52}}{6\sqrt[3]{2}} - \\ - (1 \pm i\sqrt{3})\frac{\sqrt[3]{2}}{6\sqrt[3]{3\sqrt{3}\sqrt{27z^2 - 104z + 100} + 27z - 52}}$$

We can show that

$$|\lambda_{2/3}|^2 = \frac{4W^4 - 16W^3 + 60W^2 - 16W + 4}{36W^2} \geq 1 \quad \text{for all } W \geq 1$$

where $W = \frac{\sqrt[3]{3\sqrt{3}\sqrt{27z^2 - 104z + 100} + 27z - 52}}{\sqrt[3]{2}} \geq 1$ for $z \geq 2$.

This proves the theorem in the case of the one dimensional diffusive scheme.

Dispersive Scheme

In this section, we prove that the one-dimensional free-space fully discrete dispersive scheme is unconditionally stable and non-dissipative. Consider applying the fully discrete dispersive scheme to $u_j^n = e^{i(\tilde{k}j\Delta x - \tilde{\omega}n\Delta t)}$. We obtain a polynomial

$$\lambda^2 + (2 - 4z)\lambda + 1 = 0$$

where $\lambda = e^{i\tilde{\omega}\Delta t}$ and $z = A(\tilde{k}, \nu)$. Note that the lemma implies $0 \leq z \leq 1$ for all $\tilde{k}$ and $\Delta x, \Delta t > 0$. We can solve to obtain the roots $\lambda_{1/2} = (2z - 1) \pm i\sqrt{(1 - z)z}$. We can show $|\lambda_{1/2}| = 1$ for all $0 \leq z \leq 1$, so the fully discrete dispersive scheme is unconditionally stable, and non-dissipative. This proves the theorem in the case of the one dimensional dispersive

scheme.

Extension to Higher Dimensions

When applying the dimensionally-split two-dimensional schemes to $u^n_{jk} = e^{i(\tilde{k}_x j\Delta x + \tilde{k}_y k\Delta y - \tilde{\omega} n\Delta t)}$, we obtain the same Von Neumann polynomials as in the 1D case, and basically the same stability analysis can be repeated. This can be easily extended to dimensionally-split schemes in any dimension.

□

This Von Neumann analysis does not take into consideration the effects of boundary conditions, and in principle, certain numerical boundary conditions could result in instability. In the test problems presented in [8, 7, 9] as well as the present work, the stability of the method seems robust under a variety of numerical boundary conditions. A stability analysis for some 1D fully discrete schemes (slightly different from those presented here) with numerical Dirichlet and Neumann boundary conditions was carried out in [8], showing unconditional stability in those schemes. A similar stability analysis could also be carried out for the schemes considered in this work to study the stability of these schemes under the inclusion of numerical boundary conditions.

References

1. TD Arber and RGL Vann, *A critical comparison of eulerian-grid-based vlasov solvers*, Journal of computational physics **180** (2002), no. 1, 339–357.
2. Kiyoshi Asano and Seiji Ukai, *On the vlasov-poisson limit of the vlasov-maxwell equation*, Studies in Mathematics and Its Applications **18** (1986), 369–383.
3. Willard H Bennett, *Magnetically self-focussing streams*, Physical Review **45** (1934), no. 12, 890.
4. Charles Kennedy Birdsall and Allan Bruce Langdon, *Plasma physics via computer simulaition*, CRC Press, 2005.
5. José A Bittencourt, *Fundamentals of plasma physics*, Springer, 2004.
6. Oscar P Bruno and Mark Lyon, *High-order unconditionally stable fc-ad solvers for general smooth domains i. basic elements*, Journal of Computational Physics **229** (2010), no. 6, 2009–2033.
7. M. Causley, Y. Güçlü, E. Wolf, and A. Christlieb, *A Fast, Unconditionally stable solver for the wave equation based on the Method of Lines Transpose*, **(in preparation)**.
8. Matthew Causley, Andrew Christlieb, Benjamin Ong, and Lee Van Groningen, *Method of lines transpose: An implicit solution to the wave equation*, Mathematics of Computation (2014).
9. Matthew F Causley and Andrew J Christlieb, *Higher order a-stable schemes for the wave equation using a successive convolution approach*, SIAM Journal on Numerical Analysis **52** (2014), no. 1, 220–235.
10. Roman Chapko, Rainer Kress, et al., *Rothes method for the heat equation and boundary integral equations*, Journal of Integral Equations and Applications **9** (1997), no. 1, 47–69.
11. Guangye Chen, Luis Chacón, and Daniel C Barnes, *An energy- and charge-conserving, implicit, electrostatic particle-in-cell algorithm*, Journal of Computational Physics **230** (2011), no. 18, 7018–7036.
12. Chio-Zong Cheng and Georg Knorr, *The integration of the vlasov equation in configuration space*, Journal of Computational Physics **22** (1976), no. 3, 330–351.
13. Andrew J Christlieb, Robert Krasny, John P Verboncoeur, Jerold W Emhoff, and Iain D Boyd, *Grid-free plasma simulation techniques*, Plasma Science, IEEE Transactions on **34** (2006), no. 2, 149–165.
14. Bruce I Cohen, A Bruce Langdon, and Alex Friedman, *Implicit time integration for plasma simulation*, Journal of Computational Physics **46** (1982), no. 1, 15–38.
15. Lawrence C. Evans, *Partial differential equations*, 2nd ed ed., Graduate studies in mathematics, vol. v. 19, American Mathematical Society, Providence, R.I., 2010.

16. Francis Filbet and Eric Sonnendrücker, *Comparison of eulerian vlasov solvers*, Computer Physics Communications **150** (2003), no. 3, 247–266.
17. Matthew R Gibbons and Dennis W Hewett, *The darwin direct implicit particle-in-cell (dadipic) method for simulation of low frequency plasma phenomena*, Journal of Computational Physics **120** (1995), no. 2, 231–247.
18. Roger W Hockney and James W Eastwood, *Computer simulation using particles*, CRC Press, 1988.
19. Mary Catherine A Kropinski and Bryan D Quaife, *Fast integral equation methods for rothe's method applied to the isotropic heat equation*, Computers & Mathematics with Applications **61** (2011), no. 9, 2436–2446.
20. _____, *Fast integral equation methods for the modified helmholtz equation*, Journal of Computational Physics **230** (2011), no. 2, 425–434.
21. Lev Davidovich Landau and Evgenii Mikhailovich Lifshitï¸ sï¸¡, *The classical theory of fields*, vol. 2, Butterworth-Heinemann, 1975.
22. A Bruce Langdon, Bruce I Cohen, and Alex Friedman, *Direct implicit large time-step particle simulation of plasmas*, Journal of Computational Physics **51** (1983), no. 1, 107–138.
23. Jongwoo Lee and Bengt Fornberg, *Some unconditionally stable time stepping methods for the 3d maxwell's equations*, Journal of Computational and Applied Mathematics **166** (2004), no. 2, 497–523.
24. Peijun Li, Hans Johnston, and Robert Krasny, *A cartesian treecode for screened coulomb interactions*, Journal of Computational Physics **228** (2009), no. 10, 3858–3868.
25. Mark Lyon and Oscar P Bruno, *High-order unconditionally stable fc-ad solvers for general smooth domains ii. elliptic, parabolic and hyperbolic pdes; theoretical considerations*, Journal of Computational Physics **229** (2010), no. 9, 3358–3381.
26. PJ Mardahl and JP Verboncoeur, *Charge conservation in electromagnetic pic codes; spectral comparison of boris/dadi and langdon-marder methods*, Computer physics communications **106** (1997), no. 3, 219–229.
27. Martin Masek and Paul Gibbon, *Mesh-free magnetoinductive plasma model*, Plasma Science, IEEE Transactions on **38** (2010), no. 9, 2377–2382.
28. Takefumi Namiki, *3-d adi-fdtd method-unconditionally stable time-domain algorithm for solving full vector maxwell's equations*, Microwave Theory and Techniques, IEEE Transactions on **48** (2000), no. 10, 1743–1748.
29. Donald W Peaceman and Henry H Rachford, Jr, *The numerical solution of parabolic and elliptic differential equations*, Journal of the Society for Industrial & Applied Mathematics **3** (1955), no. 1, 28–41.
30. SV Petropavlovsky and SV Tsynkov, *Quasi-lacunae of maxwell's equations*, SIAM Journal on Applied Mathematics **71** (2011), no. 4, 1109–1122.
31. E Pohn, Magdi Shoucri, and G Kamelander, *Eulerian vlasov codes*, Computer physics communications **166** (2005), no. 2, 81–93.
32. RJ Procassini, CK Birdsall, and EC Morse, *A fully kinetic, self-consistent particle simulation model of the collisionless plasma–sheath region*, Physics of Fluids B: Plasma Physics (1989-1993) **2** (1990), no. 12, 3191–3205.
33. Erich Rothe, *Zweidimensionale parabolische randwertaufgaben als grenzfall eindimensionaler randwertaufgaben*, Mathematische Annalen **102** (1930), no. 1, 650–670.
34. Jack Schaeffer, *The classical limit of the relativistic vlasov-maxwell system*, Communications in mathematical physics **104** (1986), no. 3, 403–421.
35. David N Smithe, John R Cary, and Johan A Carlsson, *Divergence preservation in the adi algorithms for electromagnetics*, Journal of Computational Physics **228** (2009), no. 19, 7289–7299.
36. Alen Taflove and Susan C Hagness, *Computational electrodynamics: the fdtd method*, Artech House Boston, London (2000).
37. John P Verboncoeur, *Aliasing of electromagnetic fields in stair step boundaries*, Computer physics communications **164** (2004), no. 1, 344–352.
38. _____, *Particle simulation of plasmas: review and advances*, Plasma Physics and Controlled Fusion **47** (2005), no. 5A, A231.
39. Kane S Yee, *Numerical solution of initial boundary value problems involving maxwell's equations*, IEEE Trans. Antennas Propag **14** (1966), no. 3, 302–307.

40. Fenghua Zhen, Zhizhang Chen, and Jiazong Zhang, *Toward the development of a three-dimensional unconditionally stable finite-difference time-domain method*, Microwave Theory and Techniques, IEEE Transactions on **48** (2000), no. 9, 1550–1558.
41. Fenghua Zheng, Zhizhang Chen, and Jiazong Zhang, *A finite-difference time-domain method without the courant stability conditions*, Microwave and Guided Wave Letters, IEEE **9** (1999), no. 11, 441–443.

Department of Mathematics, Michigan State University, East Lansing, MI 48824
E-mail address: christli@msu.edu

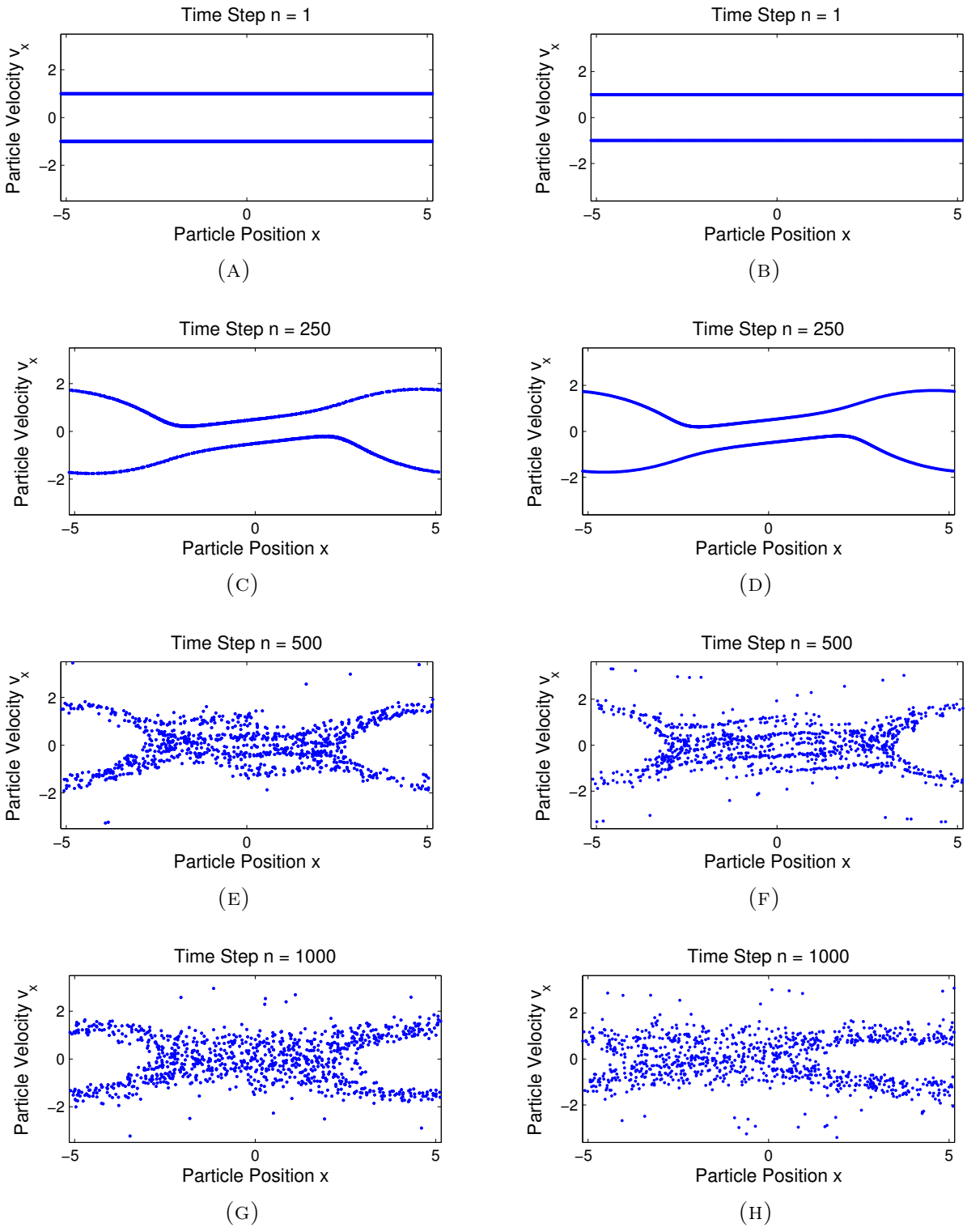

FIGURE 5. We see selected particle phase space plots for the two stream instability problem. The left column is from the 1D simulation, while the right column is from the 2D simulation, following a fixed slice of particles initialized along the line $y = -L_y/2$.

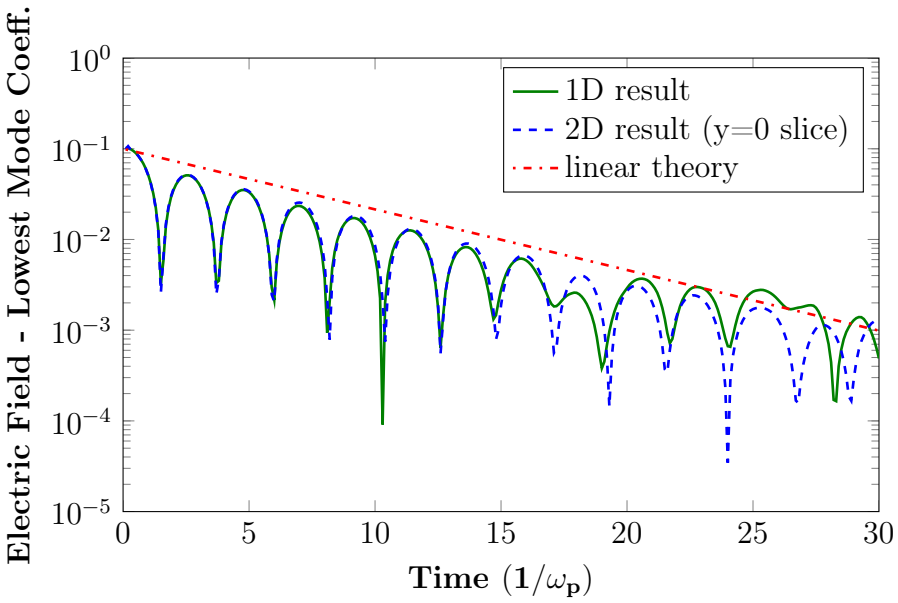

FIGURE 6. Landau damping of the lowest mode, corresponding to $k = 0.5$. Green is the 1D numerical result, blue is the 2D numerical result (measured along the central $y = 0$ slice), and red is the prediction of linear theory. We see that the correct decay rate is reproduced in our simulations

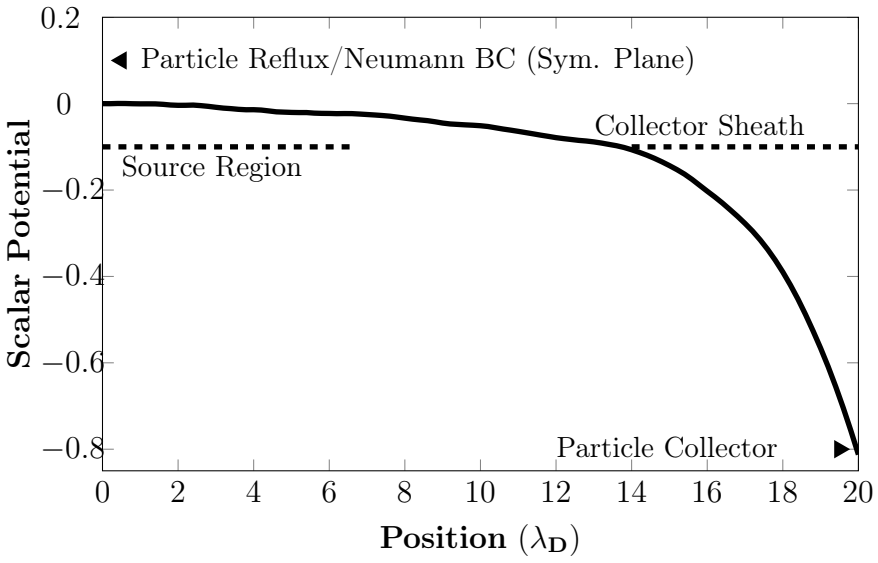

(A)

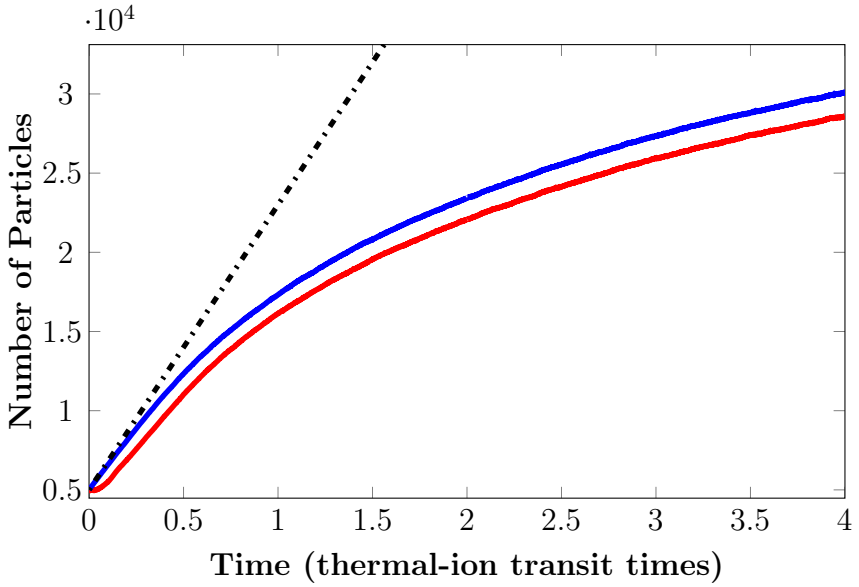

(B)

FIGURE 7. In 7a, we see the scalar potential profile at $t = 3.6$ thermal-ion transit times. In 7b, we see the simulation electron and ion count, the red and blue curves respectively, along with the injection rate, the black dashed line.

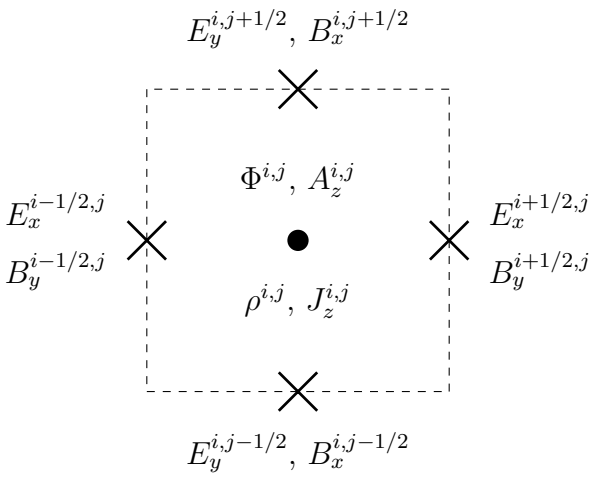

FIGURE 8. The staggered grid used for the Bennett pinch problem.

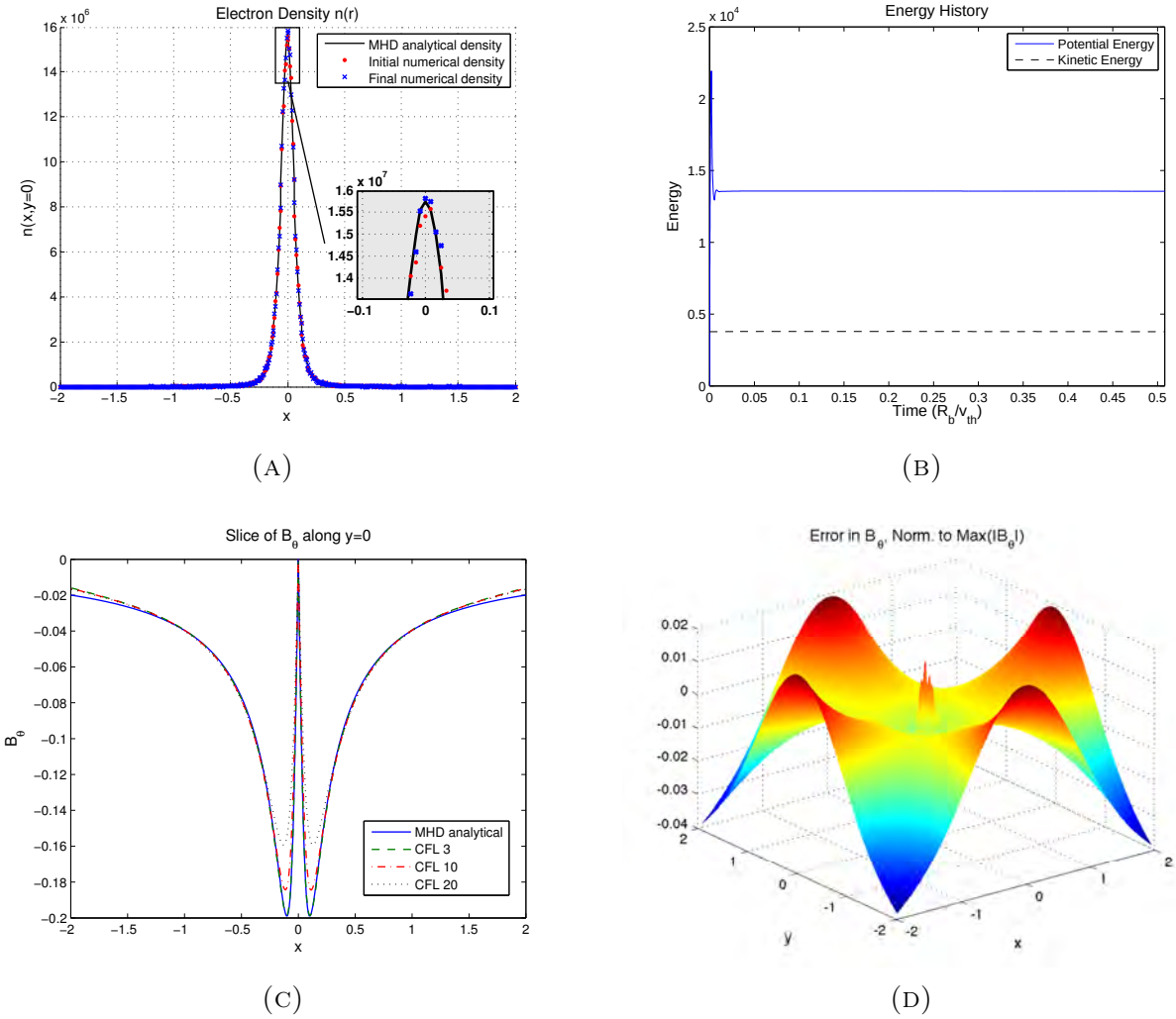

(A) (B)

(C) (D)

FIGURE 9. The figure shows 9a electron density, 9b and potential energies, 9c magnetic field at various CFL numbers, and 9d the relative error in the azimuthal magnetic field B_θ (normalized to the maximum value of the magnetic field). Results are with a CFL number of 3, except as noted in 9c. Position units are in terms of effective beam radius R_b.

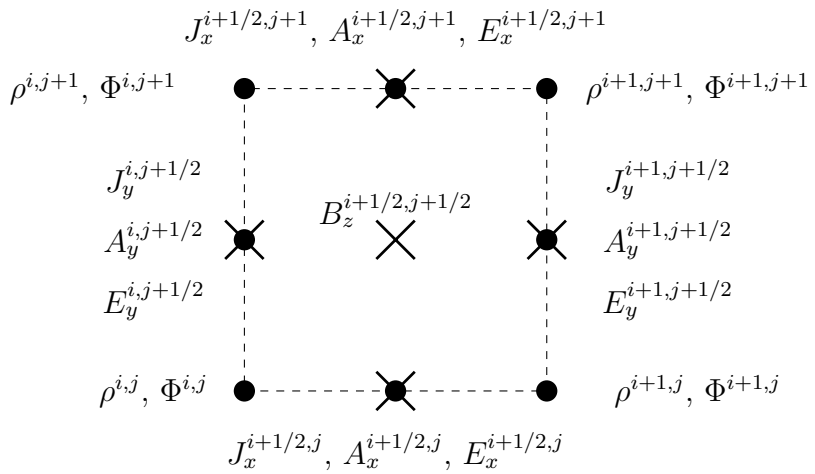

FIGURE 10. The staggered grid used for the Mardahl beam problem.

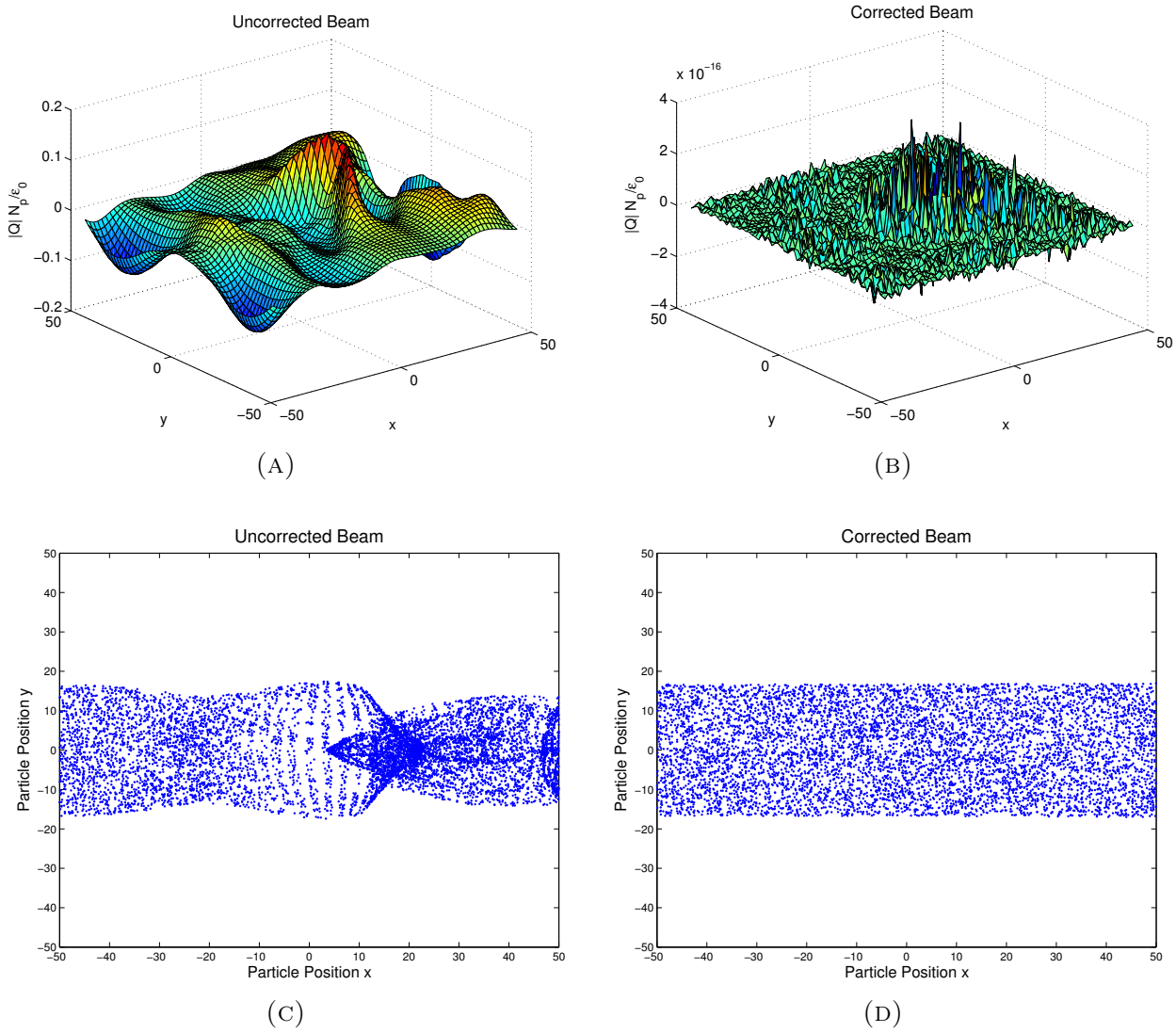

FIGURE 11. The figure shows the divergence error in the electric fields and the final beam distribution calculated from a wave equation potential 11a, 11c and in the Poisson equation potential 11b, 11d.

1.

1. Report Type

Final Report

Primary Contact E-mail

Contact email if there is a problem with the report.

christli@msu.edu

Primary Contact Phone Number

Contact phone number if there is a problem with the report

517-353-3831

Organization / Institution name

Michigan State University

Grant/Contract Title

The full title of the funded effort.

Method of Lines Transpose an Implicit Vlasov Maxwell Solver for Plasmas

Grant/Contract Number

AFOSR assigned control number. It must begin with "FA9550" or "F49620" or "FA2386".

FA9550-11-1-0281

Principal Investigator Name

The full name of the principal investigator on the grant or contract.

Andrew Christlieb

Program Manager

The AFOSR Program Manager currently assigned to the award

Fariba Fahroo

Reporting Period Start Date

06/01/2010

Reporting Period End Date

01/01/2015

Abstract

We present a new particle-in-cell (PIC) method for the simulation of plasmas based on a recently developed, unconditionally stable solver for the wave equation. This method is not subject to a CFL restriction, limiting the ratio of the time step size to the spatial step size, typical of explicit methods, while maintaining computational cost and code complexity comparable to such explicit schemes. We describe the implementation in one and two dimensions for both electrostatic and electromagnetic cases, and present the results of several standard test problems, showing good agreement with theory with time step sizes much larger than allowed by typical CFL restrictions.

Distribution Statement

This is block 12 on the SF298 form.

Distribution A - Approved for Public Release

Explanation for Distribution Statement

If this is not approved for public release, please provide a short explanation. E.g., contains proprietary information.

DISTRIBUTION A: Distribution approved for public release.

SF298 Form

Please attach your SF298 form. A blank SF298 can be found here. Please do not password protect or secure the PDF The maximum file size for an SF298 is 50MB.

AFD-070820-035 copy.pdf

Upload the Report Document. File must be a PDF. Please do not password protect or secure the PDF . The maximum file size for the Report Document is 50MB.

AFOSR_REOPORT_Christlieb_4_14_2015.pdf

Upload a Report Document, if any. The maximum file size for the Report Document is 50MB.

Archival Publications (published) during reporting period:

1. J. Qiu and A.J. Christlieb, “A Conservative high order semi-Lagrangian method for the Vlasov Equation”, Journal of Computational Physics, 229(4), 1130–1149, 2010.

2. A.J. Christlieb, C.B. Macdonald and B. Ong, “Parallel High-Order Integrators”, SIAM Jour- nal on Scientific Computing, 32, 818–835, 2010.

3. S. Olson, A.J. Christlieb and Fredrik Fatemi, “PID feedback for load-balanced parallel grid- less DSMC”, Computer Physics Communications, issn 0010-4655, 2010.

4. A.J. Christlieb and B. Ong, “Implicit Parallel Time Integrators”, Journal of Scientific Com- puting, issn 0885–7474, 2010.

5. A.J. Christlieb, M. Morton, B. Ong and J. Qiu, “Semi-Implicet Integral Deferred Correction Constructed with High Order Additive Runge-Kutta Methods”, Communications in Mathe- matical Sciences 9(3), 879–902, 2011

6. C. Shen, J. Qiu and A.J. Christlieb, “High Order Adaptive Mesh Refinement Based on Weighted Essentially Non-Oscillatory Schemes”, Journal of Computational Physics, 230(10), 3780–3802, 2011

7. N. Gavish, J. Jones, Z. Xu, A.J. Christlieb and K. Promislow, “Variational Models of Net- work Formation and Ion Transport: Applications to Perfluorosulfonate Ionomer Membranes”, Polymers, 4(1), 630–655, 2012

8. A.J. Chirstlieb, K. Promislow and Z. Xu “On the unconditionally gradient stable scheme for Cahn-Hilliard equation and its implementation with Fourier method”, Communications in Mathematical Sciences 11(2),345–360, 2012

9. A.J. Christlieb, R Haynes, B. Ong, “A Parallel Space-Time Algorithm”, SIAM Journal on Scientific Computing, SIAM J. on Scientific Computing, 34(5):233-248, 2012

10. D. Lawlor, Y. Wang, and A.J. Christlieb, “Adaptive Sub-Linear Time Fourier Algorithms”, Advances in Adaptive Data Analysis, 5(01), 2013

11. K. Promislow, J. Jones, Z. Xu, N. Gavish and A.J. Christlieb, “Variational Models of Pore Networks in Ionomer Membranes: The Role of Electrostatics”, ECS Transactions, 50(2), 161–173, 2013

12. M.CausleyandA.J.Christlieb,“A-StableHigherorderschemesforthewaveequationusing a recursive convolution approach” , SIAM Journal on Numerical Analysis, 52(1), 220–235, 2014

13. Y. Cheng, A.J. Christlieb, X. Zhong, “Energy-conserving discontinuous Galerkin methods for the Vlasov Ampere system ”, Journal of Computational Physics, 256, 630–655, 2014

14.A.J.Christlieb,J.Jones,K.Promislow,B.Wetton,M.Willoughby,“Highaccuracysolutions to energy gradient flows from material science models”, Journal of Computational Physics, 257, Part A, 193–215, 2014

15. A.J. Christlieb, W. Guo, M. Mortion and J. Qiu, “A High Order Time Splitting Method Based on Integral Deferred Correction for Semi-Lagrangian Vlasov Simulations”, Journal of Computational Physics, 267, 7–27, 2014

16. M. Causley, A.J. Christlieb, B. Ong, L. VanGroningen, “Method of Lines Transpose: An Implicit Solution to the One Dimensional Wave Equation” , AMS – Mathematics of Compu- tation, 83, 2763–2786, 2014

17. A.J. Christlieb, Y. Guclu, D. Seal, “High-order multiderivative time integrators for hyper- bolic conservation laws”, Journal of Scientific Computing, 60 (1), 101–140, 2014

18. A.J. Christlieb, J.A. Rossmanith, Q. Tang, “Finite Difference Weighted Essentially Non- Oscillatory Schemes with Constrained Transport for Ideal Magnetohydrodynamics”, Journal of Computational Physics, 268, 302–325, 2014

19. T. Xiong, J. Qiu, Z. Xu, A. Christlieb, “High Order Maximum Principle Preserving Semi-Lagrangian Finite Difference WENO schemes for the Vlasov Equation”, Journal of Compu- tational Physics, 273, 618–639, 2014

20. S. Olson, G. Raithel and A.J. Christlieb “Pressure-Driven Evaporative Cooling in Atom Guides”, in Physical Review A, 90, 043612, 2014

21. Y. Gucly, A.J. Christlieb, W.N.G. Hitchon, “Arbitrarily high order Convected Scheme so- lution of the Vlasov-Poisson systemr”, Journal of Computational Physics, 270, 711–752, 2014

22. Y. Cheng, A.J. Christlieb, X. Zhong, “Energy-conserving Discontinuous Galerkin Methods for the Vlasov-Maxwell System”, Journal of Computational Physics, 279, 145–173, 2014

Changes in research objectives (if any):

We found a fast way to develop the implicit solver based on a splitting approach we would have not guessed from the onset. The A-stable method is now as fast as an explicit time stepping approach! We were also able to combined the method with a PIC time method for solving the Vlasov Maxwell system.

Change in AFOSR Program Manager, if any:

NA

Extensions granted or milestones slipped, if any:

NA

AFOSR LRIR Number

LRIR Title

Reporting Period

Laboratory Task Manager

Program Officer

Research Objectives

Technical Summary

Funding Summary by Cost Category (by FY, $K)

	Starting FY	FY+1	FY+2
Salary			
Equipment/Facilities			
Supplies			
Total			

Report Document

Report Document - Text Analysis

Report Document - Text Analysis

Appendix Documents

2. Thank You

E-mail user

Apr 12, 2015 14:43:22 Success: Email Sent to: christli@msu.edu